Convective Interaction with Dynamics in a Linear Primitive Equation Model*

RICHARD SEAGER**

Joint Institute for Study of the Atmosphere and Ocean, University of Washington, Seattle, Washington

STEPHEN E. ZEBIAK

Lamont–Doherty Earth Observatory of Columbia University, Palisades, New York

(Manuscript received 19 May 1993, in final form 13 October 1993)

ABSTRACT

A new global atmosphere model purpose designed for climate studies is introduced. The model is solved in terms of the normal modes of the linearized primitive equations on a sphere, which allows use of long time steps without introducing computational instability or phase errors of the linear wave components. The model is tested by attempting to simulate the tropical intraseasonal oscillation using an idealized sea surface temperature distribution. Simple treatments of radiation and boundary-layer processes are used together with the much more complete Betts–Miller convection scheme. The Betts–Miller scheme maintains the atmosphere in a state of near neutrality to reversible saturated ascent. It is found that for different values of the surface evaporation time scale, either the evaporation–wind feedback mechanism postulated by Neelin et al. and Emmanuel or low-level convergence of moisture can create eastward propagating deep convective modes. In general, both mechanisms seem important, but it is the latter mechanism that provides phase speeds more in line with observations. Moisture convergence in this model works to erode the low-level equivalent potential temperature inversion that is ubiquitous in nonconvecting regions, thus triggering convection. In contrast to CISK models, changes in boundary-layer equivalent potential temperature are essential in this model to create propagating modes.

The primary deficiency of the model is the tendency of the model to favor horizontal scales of convective disturbances that are much smaller than the zonal wavenumber one or two disturbances observed. This is related to the absence in the model of any pulsation of convection on an intraseasonal time scale over the warmest water regions that has been observed in satellite OLR data. Possible reasons for these differences are discussed.

1. Introduction

The large-scale motions of the tropical atmosphere are observed to be thermally direct circulations. Over most of the tropical regions radiative cooling to space is balanced by adiabatic warming due to subsidence. In more geographically confined regions deep convection occurs and the resulting latent heating plus radiative cooling is balanced by adiabatic cooling due to ascent. This horizontal variation in diabatic heating creates temperature and pressure gradients such that horizontal motion connects the regions of descent and ascent. At the surface, fluxes of moisture and heat provide the energy required to maintain these circulations against frictional dissipation and radiative damping.

It is quite striking that the regions of convection, and hence upward motion, are more confined than the regions of descent. This is commonly accepted to result from an interaction between the dynamic response to diabatic forcing and the forcing itself. Charney and Eliassen (1964) introduced the term *conditional instability of the second kind* (CISK) to describe a theory for how this cooperation works. Central to their concept was the idea that surface friction could indirectly act as an energy source for a developing disturbance. This is because the friction induces convergent inflow to the center of the disturbance that increases the supply of moisture to the disturbance. Precipitation and latent heating will increase in response thus strengthening the disturbance. That in turn will lead to increased moisture convergence at low levels providing an interaction between "simple gravitational instability in a moist environment on the one hand, and with the frictionally driven, cooperative, depression-cumulus system on the other" (Charney and Eliassen 1964, p. 74). Also central to the theory was the then common assumption that the atmosphere was conditionally unstable to moist convection. This meant that convection, by reducing

* Contribution Number 230 of the Joint Institute for Study of the Atmosphere and Ocean and Number 5132 of Lamont–Doherty Earth Observatory.

** Current affiliation: NOAA Program in Climate and Global Change Visiting Post-Doctoral Fellow, Lamont–Doherty Earth Observatory of Columbia University, Palisades, New York.

Corresponding author address: Dr. Richard Seager, Lamont–Doherty Earth Observatory, Palisades, NY 10964.

the potential energy in the column, created an energy source that could be tapped by the large-scale circulation.

Since its original implementation as an explanation for deepening of hurricanes, CISK has been employed extensively as an explanation for other tropical phenomena that involve convection. Charney (1971) and Schneider and Lindzen (1977) used CISK as an explanation for the formation of the intertropical convergence zone (ITCZ). Lau and Peng (1987), Sui and Lau (1989), Swinbank et al. (1988), and Hayashi and Sumi (1986), among others, have used CISK to explain the existence and eastward propagation of the 30–60 day oscillation in the atmosphere. Kuo (1974) developed a convective parameterization scheme that is widely used in general circulation models (GCMs) that explicitly invokes CISK by only allowing convection to occur in regions of moisture convergence. Convergence-dependent heating has also been used in simple models of interannual variability (e.g., Zebiak 1986) although in this case the rationale was little more than the observed correlation between low-level convergence and convective heating.

Recently the commonly held assumption that the mean tropical atmosphere is conditionally unstable has come into question. Betts (1982), while accepting the instability relative to a moist adiabat, noted the correspondence between observed atmospheric profiles and a *virtual* moist-adiabatic lapse rate. The difference between the two is that the virtual moist adiabat takes into account the effect on buoyancy of the condensed vapor, whereas a moist adiabat assumes condensate immediately rains out. Xu and Emanuel (1989) analyzed numerous tropical profiles and found that, except for those profiles that were stable, the atmosphere did indeed approximate to a virtual moist adiabat. Presumably this is not a coincidence. Convecting towers probably do carry their condensate to at least some level so the appropriate adiabat is a reversible virtual adiabat rather than the irreversible moist adiabat. The observed near neutrality of the atmosphere to moist convection is then the result of rapid convective release of conditional instability whenever it appears. This is also a more satisfactory view of the tropical atmosphere than the assumption that it is conditionally unstable everywhere, since the latter theory cannot explain what it is that prevents all this convectively available potential energy from being released.

If the atmosphere is indeed either stable or near neutral to moist convection, and we believe that this is the case, then convection cannot act to effect a significant transfer of potential energy to kinetic energy since the atmospheric state is always one of near zero convective available potential energy (CAPE). The central point is that CISK cannot work in an atmosphere that is not conditionally unstable. This casts doubt on the convection parameterizations in many GCMs and on the explanations of several tropical phenomena involving convection. If the atmosphere was neutrally stable, intensification of disturbances would rely critically on surface fluxes and convection would perform the role of communicating the perturbations in boundary-layer moist entropy to the rest of the atmospheric column. The large-scale dynamics would then respond to the rearrangement of atmospheric mass that surface fluxes and convection create. In contrast to the CISK scenario, in this case there is no alteration in the free atmosphere temperature (and hence pressure distribution) unless the boundary-layer moist entropy changes. In recognition of this range of possible interactions, and to avoid further confusion from use of the term CISK, Neelin and Yu (1993) have suggested the term "convective interaction with dynamics" (CID) to cover all the possibilities.

The two most commonly used convection parameterizations in atmosphere models are the Kuo scheme and moist convective adjustment. The former allows convection to occur only if certain conditions in addition to gravitational instability are met. The strongest conditions relate to the requirement for moisture convergence into the column and a requirement for a threshold relative humidity to be exceeded. If these (and possibly other) conditions are met, the convective tendencies of temperature and humidity are computed using a simplified cloud model. In moist convective adjustment the atmosphere is instantaneously adjusted to a moist (irreversible) adiabat if the column is unstable and if the low-level relative humidity exceeds some threshold value. There is no convergence criterion. As Emanuel (1988) has pointed out, both these schemes, by disallowing convection when the atmosphere is unstable but the auxiliary conditions are not fulfilled, allow the buildup of conditional instability. Models with these schemes can then be expected to exhibit CISK-like behavior.

In nature convection occurs as a response to a gravitational instability and is not in any way dependent on the presence of auxiliary conditions such as moisture convergence. It is sometimes argued that large-scale convergence is required in order to force vertical ascent such that a negatively buoyant unsaturated parcel can be forced to its lifting condensation level and become positively buoyant. However, in the real atmosphere there is normally sufficient turbulent mixing to accomplish this lifting. Indeed, over large areas of the subtropics convection does occur, albeit shallow, even though large-scale moisture divergence and subsident motion prevail. The convection scheme developed by Arakawa and Schubert (1974) does not rely on extraneous conditions but is complex and not widely used in atmospheric models. So-called mass flux schemes may also use moisture convergence for a closure scheme (e.g., Tiedtke 1989). Recently two other convection schemes that work solely on buoyancy criteria have been developed, the first by Betts and Miller

(1986) and Betts (1986) and the second by Emanuel (1991).

Emanuel's scheme rests on an explicit treatment of subcloud-scale updrafts and downdrafts, which ascend and descend according to their buoyancy. In one-dimensional radiative–convective calculations this scheme has been shown to perform well and reproduce some desirable features, such as the trade wind inversion and trade cumulus clouds; however, it is yet to be fully tested in a three-dimensional numerical model. The Betts–Miller scheme adopts a more empirical and much simpler approach that relaxes model temperature and humidity profiles over a finite time scale to observed profiles derived from moist virtual adiabats. Betts (1986) presented one-dimensional calculations for a wide variety of regimes (polar as well as tropical) that showed a very impressive agreement with observations. Neelin and Yu (1993) used a simplified version of this scheme in a simple analytical model. The scheme has gained some popularity recently. It has been implemented in the National Meteorological Center's (NMC) ETA coordinate prediction model as described by Janjić (1990), who reported a satisfactory performance. Slingo et al. (1993) discuss its use in a simulation of tropical precipitation and circulation in the U.K. Universities Global Atmospheric Modeling Program GCM, which is derived from the European Centre for Medium-Range Weather Forecasts (ECMWF) model. They compared the results with simulations performed with the Kuo scheme and found that the Betts–Miller scheme led to more confined areas of precipitation and more organized propagating convective systems. It is quite interesting that the Kuo scheme, although it is dependent on moisture convergence, which is frequently cited as the explanation for the limited spatial scale of convection, led to a simulation with more diffuse regions of precipitation than the Betts–Miller scheme, which contains no such dependence. Ji et al. (1993, personal communication) report a similar experience with the Kuo scheme in the standard NMC global model.

In this paper we will present some results obtained using the Betts–Miller scheme in a linear version of a new global atmosphere model that has been purposely designed for climate studies. We will focus on the 30–60 day oscillation since that is a reasonable phenomenon with which to test the range of convective interaction with dynamics possible in this model. To date most explanations of this phenomenon have invoked CISK. However, Neelin et al. (1987) and Emanuel (1987) have suggested that it is instead affected by, or even driven by, zonal asymmetries in surface fluxes induced by the winds contained within the oscillation. To date the extent to which model representations of the 30–60 day oscillation depend on the model's convection scheme is unclear. The extent to which surface fluxes and moisture convergence contribute to the existence of the oscillation and its eastward propagation is also unknown. Unfortunately, it is also doubtful whether any of the model realizations of the oscillation are very realistic. Some answers to these questions will be offered here, but not without raising new questions.

In the next section we will introduce the dynamical model and describe the Betts–Miller convection scheme. In section 3 we will present a brief description of observed features of the 30–60 day oscillation. In section 4 we will show a model simulation of the oscillation using a simplified convergence-dependent heating. In section 5 we will present results using the Betts–Miller convection scheme. A discussion of implications and conclusions will follow in section 6.

2. Model description

a. *Dynamics*

The dynamical model used in this study has recently been developed for application to problems in medium and long-term climate variability. We have attempted to devise a model that is accurate and general but is also computationally efficient so as to allow long-term integrations. To this end a new method of solution of the primitive equations has been developed. The model equations are presented and discussed in detail in the Appendix. Here we will briefly describe the main characteristics of the model.

We begin with the primitive equations in spherical coordinates discretized on a vertical grid in such a way as to conserve energy. We linearize about a state of no motion, and obtain the normal modes (eigensolutions) of the linear system. A vertical structure equation is derived from the combined continuity and thermodynamic equations by assuming the solution is separable in the vertical and horizontal. The vertical structure equation is solved by standard numerical procedures to yield as many vertical eigenfunctions and accompanying eigenvalues as there are vertical layers in the system. For certain choices of the differencing of the hydrostatic equation, and enforcing consistency with that choice throughout the system, the vertical eigenfunctions are orthogonal. This procedure is very similar to those adopted in normal-mode initialization (in particular, see Temperton 1984).

Vertical normal-mode decomposition reduces the original N-layer system to N shallow-water systems, each with an equivalent depth that is proportional to the corresponding eigenvalue of the vertical structure equation. We now seek the normal modes of the shallow-water systems. Following methods outlined by Kasahara (1976, 1978), we use a spherical harmonic expansion to derive a matrix eigenvalue problem for each zonal wavenumber. The eigenvectors of these matrices provide coefficients in the spherical harmonic expansion for the normal modes. These normal modes are commonly referred to as Hough modes. If the series is truncated then approximations to the Hough modes can

be obtained. The eigenvalues are the oscillation frequencies of the modes. The Hough modes are guaranteed to be orthogonal to all others whatever the truncation used in the spherical harmonic expansion and for any equivalent depth. They also form a complete basis set for the discretized linear system.

After this stage the entire set of normal modes has been computed. The three-dimensional velocity and pressure structures of these modes are discretized onto a Gaussian grid (the resolution of which is chosen so as to preserve the orthogonality of the modes when evaluated under Gaussian quadrature), saved, and read in at the beginning of each run. The linear primitive equations have now been reduced to a set of ordinary differential equations describing the time evolution of the amplitude of each mode in terms of the frequency of the mode and the forcing on the mode. These amplitude equations can be solved analytically, are unconditionally stable, and do not introduce computational dispersion or phase errors of the linear waves they describe. Forcings (i.e., physics, nonlinear, and nonhomogenous terms) are evaluated in physical space and projected onto each of the orthogonal normal modes. Since forcing terms in general will depend on the modal amplitudes, this is not a purely analytical method. The forcings should evolve in tandem with the modal amplitudes, but the solution method requires that the forcings be constant for the duration of the time step. This requirement permits the amplitude equations to be solved by analytical methods, but of course, the solution is a numerical one. Once the modal amplitudes are known, inverse transforms are performed to regain model variables in physical space.

The reduction of the full system to a set of ordinary differential equations allows the choice of model time step to be decided on the basis of the application, rather than have it dictated by stability considerations. For example, for climate purposes we hope we do not have to be concerned with hour-to-hour variability. Hence, we filter out the fastest modes in the system and use a one-day time step. Processes that do evolve on a shorter time scale than one day (e.g., convection) will then require a special treatment to derive daily average forcings for the model. Clearly long time steps, while not effecting computational stability, can reduce accuracy. However, some of the experiments to be described were also performed with a 1.5-hour time step, and the results were found to be very similar. Although this partly results from the filtering out of the fastest waves, it is nonetheless encouraging.

In this study we use a six-layer version of the model. The model is formulated in sigma coordinates. There are four layers with a sigma thickness of 0.2 overlying two layers with a sigma thickness of 0.1 immediately above the surface. A Rayleigh friction is used and the model's temperature anomalies are subjected to a Newtonian cooling. In the lowest atmosphere layer a larger Rayleigh friction is applied. Because Newtonian cooling alone cannot approximate observed cooling profiles (in particular the near surface maximum) a radiative cooling profile is also imposed that increases steadily from zero in the top layer (about 100 mb) to -1.5 K/day in the lowest layer. This is designed to mimic the observed radiative cooling. For purposes of the convection routine a one-dimensional humidity equation is adopted. The humidity is calculated in physical space, accounting for vertical advection of the mean and perturbation humidity (computed with a modified upwind difference scheme), evaporation, and convective precipitation. Nonlinear vertical advection of temperature is also included to ensure that the advected thermodynamic structure is the one produced by the convection scheme and not just the basic state. A weak background vertical diffusion of temperature and humidity is also applied. The time integration is done using a time-splitting method. The modal amplitudes are first advanced subject to no forcing, and daily mean model fields are computed. The model then uses these first-guess fields for calculation of physics (convection, radiation) and calculation of the nonlinear advection of temperature. These forcings are projected onto the modes and the modal amplitudes are then advanced again from their original initial condition but now subject to the forcings. This is designed to increase the accuracy of the time integration by "centering" the forcings in time.

The evaporation–wind feedback postulated as important to the intraseasonal oscillation by Neelin et al. (1987) and Emanuel (1987) relies on the existence of equatorial mean easterlies. However, a linear model can only give zero mean easterlies on the equator. Hence, for the calculation of surface fluxes alone, we assume a mean easterly wind of 4 m s^{-1}. The fluxes are calculated with bulk formulas. It is assumed the fluxes are partially mixed throughout the lowest two atmospheric layers. Since the quantities entering the bulk formulas are at about 950 mb, rather than near surface values, the exchange coefficients must be reduced accordingly (Fissel et al. 1977). We use a value of 0.0004. At low wind speeds the exchange coefficient should increase with decreasing wind speed (e.g., Liu et al. 1979) such that the fluxes never approach zero. To account for this without having to compute the exchange coefficient, we make use of the commonly used parameterization, which enforces a minimum wind speed in the bulk formulas. In the standard cases we assume this is 3.5 m s^{-1}. This is unfortunately a crude approximation, but only a much more complex treatment of boundary-layer processes would enable a more reliable parameterization. It should be remembered, however, that models are sensitive to the treatment of fluxes in low wind speed conditions (e.g., Miller et al. 1992).

b. Convection

The convection parameterization we adopt is that of Betts (1986) and Betts and Miller (1986). This scheme

is a more sophisticated variation on moist convective adjustment and does not seek to explicitly model the cloud-scale or subcloud-scale processes that in reality determine convective forcings. To paraphrase Betts (1986), the scheme rests on the observation that a quasi equilibrium exists between the cloud field and the large-scale forcing such that, on large space and time scales, convective regions are characterized by specific temperature and moisture profiles. If the atmospheric column is unstable, then the moisture and temperature are relaxed to these observed quasi-equilibrium profiles on a time scale of order 2 hours. The observed profiles are close to, but not exactly, moist virtual adiabats. This procedure, though sidestepping detailed treatment of convective processes, ensures that the large-scale thermodynamic structure of the atmosphere in convecting regions remains close to that observed.

Convection occurs in this scheme whenever the atmosphere is unstable. Convective adjustment is suppressed if it would produce negative precipitation, that is, if the moisture supply is insufficient. This occurs relatively rarely. No other conditions—for example, on moisture convergence or relative humidity—are applied. This, together with relaxation to a near-neutral profile on a short time scale, prevents buildup of CAPE in the model and should prevent CISK-like behavior from becoming dominant. Hence, it is in considerable contrast to other convection schemes such as the one developed by Kuo (1974) that are moisture convergence dependent. Although this is an adjustment scheme, it is also distinct from moist convective adjustment (MCA). MCA applies an instantaneous adjustment of an unstable profile to a moist-adiabatic lapse rate, but only if the relative humidity exceeds a certain threshold. Both elements of MCA are open to doubt since the relative humidity requirement is unphysical and the observed atmospheric profile is not a moist adiabat.

The time scale for convective adjustment in this scheme is 2 hours, much shorter than the model time step of one day. To use the scheme, every time step we perform at each grid point a one-dimensional nested integration with a time step of 1.5 hours. Within this calculation the temperature and moisture evolve according to the balance of the radiation and compression (for temperature), advection (computed with the daily mean vertical velocity and first-guess temperature and humidity profiles), and the interactively computed surface and convective fluxes. Instability of the column is checked for each 1.5-hour time step and adjustment performed if necessary. At the end of the day the tendencies in temperatures and humidities due to convection and surface fluxes are applied as forcings to the dynamical model.

The internal working of the scheme is as follows. The saturation equivalent potential temperature is computed at all levels. If the saturation equivalent potential temperature, θ_{ES}, at the next to lowest model level is greater than the lowest-level equivalent potential temperature, θ_E, then no convective adjustment occurs. If instead the column is unstable, cloud top is found by locating the level at which the low-level θ_E intersects the environmental θ_{ES}. If cloud top is above 700 mb the convection is classified as deep and is otherwise classified as shallow.

If deep convection occurs, the next step is to compute the reference θ_{ES} profile between the lowest level and cloud top. The profile has a minimum θ_{ES} at the freezing level, beneath which the reference profile θ_{ES} decreases with height in proportion to the change of θ_{ES} along a moist *virtual* adiabat θ_{ESV}. Above the freezing level the reference profile θ_{ES} increases linearly in pressure back to the cloud-top value. In the low troposphere the profile is slightly unstable to the θ_{ESV} isopleth. The reference θ_{ES} profile is inverted for temperature and saturation specific humidity. The actual humidity is then computed by assuming a profile of $\mathcal{P} = p^* - p$, where p is the layer pressure, and p^* is the pressure to which air at p would have to be raised to become saturated. The $\mathcal{P}$ profile is again derived from observed profiles. After the reference profiles of temperature and specific humidity are computed, the profiles are adjusted to ensure that the moist static energy of the reference profile, integrated from cloud bottom to cloud top, equals that of the profile to be adjusted. Model temperatures and specific humidity are adjusted to the reference profiles with a time scale of 2 hours.

Shallow convection is assumed to be nonprecipitating. The treatment of shallow convection follows from the mixing line analysis of Betts (1982). A mixing line is constructed between air at the lowest level and air immediately above cloud top, and the saturation point on this line corresponding to an equal mix of air is calculated. A linear mixing line slope is constructed between the saturation point θ_E for an equal mixture of subcloud and above-cloud air and the low-level θ_E. The reference θ_{ES} profile is drawn through the low-level θ_{ES} and parallel to the mixing line. The reference profile is inverted for temperature and specific humidity using a first-guess value for $\mathcal{P}$. The temperature and humidity profiles are then adjusted to conserve enthalpy and moisture independently (and, unlike for deep convection, adjusting $\mathcal{P}$ in the process). Model profiles are adjusted to the reference profiles with a time scale of two hours.

Details of the scheme and the equations are given in Betts (1986).

3. Phase and propagation of the observed intraseasonal oscillation

Until recently, most observational studies of the intraseasonal oscillation used data that were highly filtered in time and space to extract the signal deemed to be of most interest. For example, studies often only looked at zonal wavenumber one or the first few zonal

wavenumbers. Time series have often been bandpass filtered to isolate phenomena with the 20–80-day periods. While some of these studies have been instructive, they also risk obscuring the real nature of the oscillation and its relation to the stationary features of the circulation and the seasonal cycle. In contrast, a recent paper by Weickmann and Khalsa (1990) (hereafter WK) presents an analysis of the behavior of the 30–60 day oscillation between September 1981 and April 1982 that uses raw outgoing longwave radiation (OLR) data and dynamical quantities that have been subjected only to a 5-day running mean. This affords a look at the variability of the oscillation, and its relationship to the regions of persistent convection and their seasonal migration, free of the selectivity of presentation that time and space filtering impose. The model results discussed in the next section will be subjected only to some mild smoothing and will be primarily compared with WK's observations. Hence, we will provide here a brief overview of their findings.

Figures 1a and 1b are taken from WK. Figure 1a shows the daily outgoing OLR from September 1981 to April 1982, averaged over 10 degrees of latitude centered on the equator. In Fig. 1b the corresponding longitude time diagram of the 150-mb velocity potential to which a five-day running mean has been applied is shown. The OLR envelopes from Fig. 1a have been superimposed onto Fig. 1b. It is immediately evident from Fig. 1a that the locations of equatorial convection are very geographically fixed. Three areas are seen: the dominant area over the Indian Ocean–western Pacific region and two smaller regions over Africa and South America. These regions are separated by intervening regions that are overwhelmingly free of convection.

A number of propagating features are apparent in Fig. 1a. Within the Indian Ocean–western Pacific sector a gradual eastward movement of regions of low OLR is seen. This feature has been emphasized by the OLR envelopes drawn in the figure but is in reality a rather indistinct feature. These clusters move with a phase speed of only a few meters per second and on their own would take more than 100 days to pass around the globe. Within these slowly propagating features are faster moving, shorter duration convective clusters. One example is the one through which WK have drawn the 8 m s^{-1} phase propagation line, although two good examples also occur in the early part of the OLR envelope drawn for March 1982. These features would travel around the globe in 40–60 days. Over South America only the faster moving features are seen superimposed on a general, and apparently random, pulsation of convection with a time scale of a few days or so. Over Africa no propagation is seen, only a weak day-to-day and week-to-week variability.

What is very clear from this data is that an observed 30–60-day periodicity in the Indian Ocean–western Pacific region is not determined by the time it takes for a propagating convective disturbance to make it around the world. Convection dies out over the eastern Pacific and, although there is some evidence of convective events over South America being preceded by events over the western Pacific, there is no evidence of a disturbance making it all the way around the world. However, in the Indian Ocean–western Pacific region, there does appear to be a 30–60-day periodicity. The times of more intense convection (as depicted by the OLR envelopes) are separated by relatively quiescent periods of shorter duration. The quiescent periods are approximately 30–60 days apart. It is clear from Fig. 1a that a spectral analysis of an OLR time series in this area would pick out this periodicity but would also be relatively broad, showing much variability at shorter periods as well.

Figure 1b (also from WK) shows the longitude time variation of the 150-mb velocity potential anomaly for the same time interval. Propagation is very evident in this figure. These propagating anomalies would travel around the globe typically in 15–25 days, faster than even the fast elements of the OLR field. WK suggest a link between these fields that is depicted by the line drawn on Fig. 1b. The slowly propagating large clusters of convective activity emit velocity potential anomalies (upper-level divergence) that move away from the disturbance rapidly. The return of that divergence anomaly to the Indian Ocean–western Pacific region is apparently correlated with the generation of a new convective cluster. The period of convective activity over this region is set by the combination of slow eastward propagation of a convective disturbance together with fast eastward propagation of presumably free atmospheric Kelvin waves. It is also clear from Fig. 1b that this relation is often good but does not always hold.

4. Model results

Figure 2 shows the idealized surface temperature field used in the simulations presented here that use the Betts–Miller convection scheme. Upon a zonally symmetric decrease of surface temperature from equator to pole, a zonally asymmetric component is imposed designed to mimic the observed tropical SST distribution. Near 100°E there is a large warm pool with water at about 30°C. A cold region is located at 140°W in the region of the Pacific cold tongue. Two other local maxima are placed at the longitudes of Africa and South America and are separated by relative minima of SST.

The first experiment we present, however, uses a simple convergence-dependent heating parameterization. It was found that if this was used with the SST in Fig. 2 then the simulation disintegrated into exponentially amplifying noise at the smallest scales possible. This is a common experience with CISK-like heating parameterizations (see Bladé and Hartmann 1993). Hence, for this experiment alone we reduced the SST in Fig. 2 by a uniform 3°C. The basic-state temperature was lowered by the same amount for calculation of the

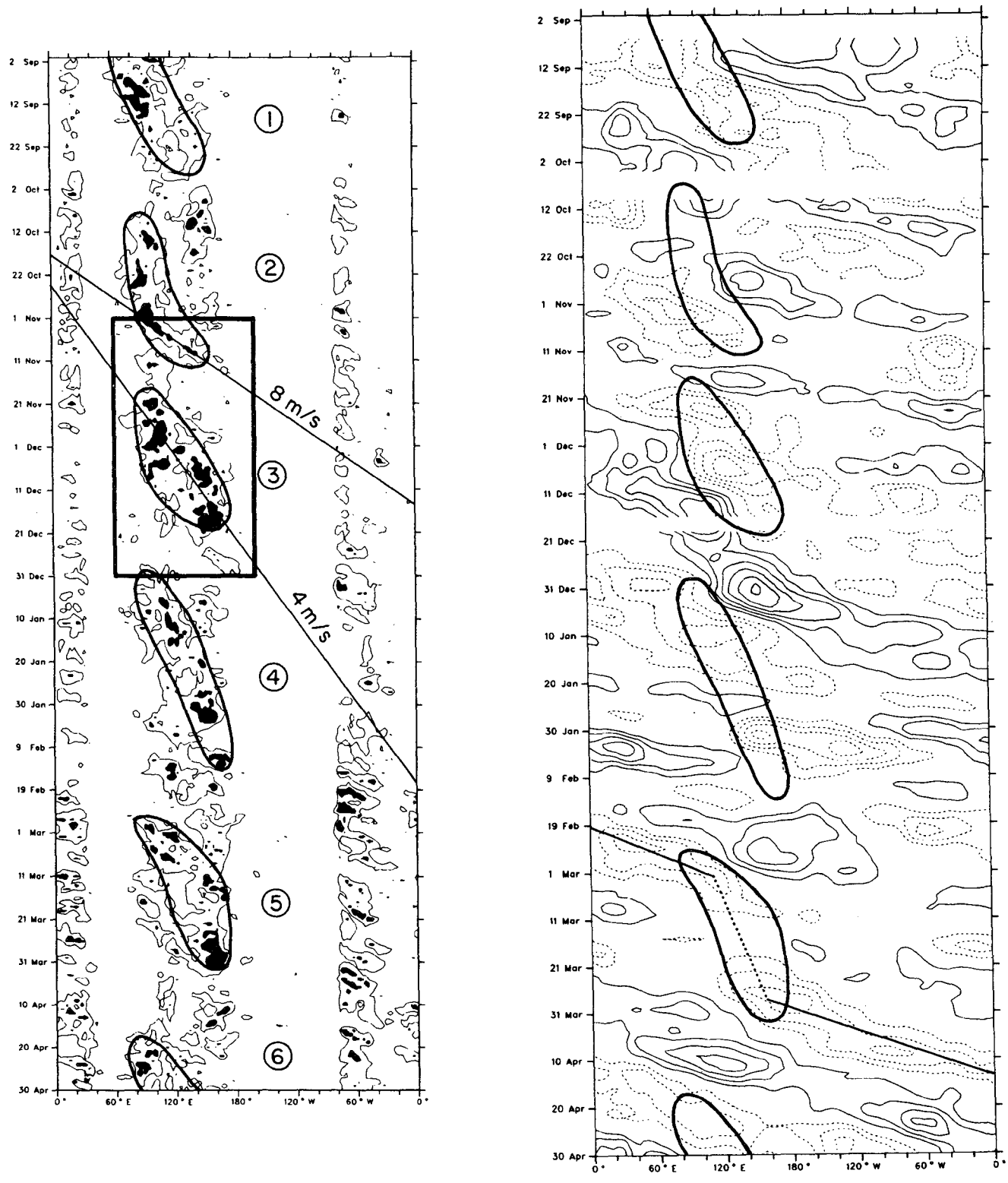

FIG. 1. (a) Hovmöller diagram of daily outgoing longwave radiation (OLR) for 1 September to 30 April 1982 averaged over 5°N–5°S. OLR $\leq$ 170 W m^{-2} is darkly shaded. (b) Hovmöller diagram of 150-mb velocity potential for same time period and averaging interval as in (a). Missing data is blank and a 5-day running mean has been applied. The contour interval is 2×10^6 m^2. The OLR envelopes from (a) have been added.

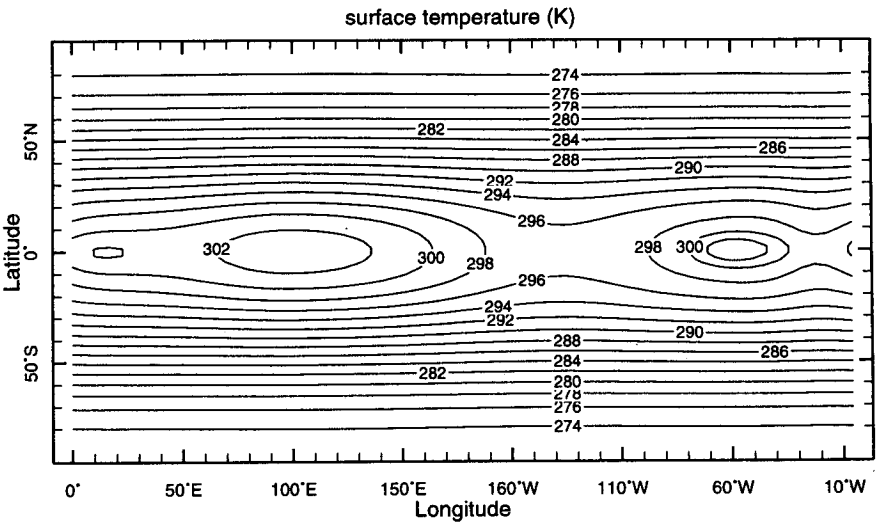

FIG. 2. Idealized sea surface temperature (K) used in model experiments with the Betts–Miller convection scheme. For the convergent-dependent heating experiment the SST was uniformly lowered by 3 K.

convergence-dependent heating only. This prevented exponential growth in most cases. It must be emphasized that no problems emerged when the more realistic SST seen in Fig. 2 was used with the Betts–Miller scheme.

a. Convergence-dependent heating

We will first present a simulation in which the convective heating of the atmosphere is proportional to the low-level moisture convergence. Over recent years several papers by K.-M. Lau and his coworkers have used such a scheme to argue that the intraseasonal oscillation is a wave–CISK mode that propagates east due to moisture convergence (Lau and Peng 1987; Sui and Lau 1989; Lau et al. 1989). As a result of the combined effects of Rossby and Kelvin waves forced by convective heating, moisture convergence maximizes to the east of the convective heating and hence provides a new convective heating center. The periodicity of the oscillation is provided by the time it takes for a propagating convective disturbance to make it around the world.

Following Lau and Peng (1987, hereafter LP), the convective heating is parameterized in regions of low-level convergence as

$$Q(\sigma) = \begin{cases} -m\eta(\sigma) rL(q_{\text{sat}}(T_5)D_5\delta\sigma_5 \\ \quad + q_{\text{sat}}(T_6)D_6\delta\sigma_6)/C_p, \\ \qquad\qquad \text{if} \quad D_5\delta\sigma_5 + D_6\delta\sigma_6 < 0 \\ 0, \qquad \text{if} \quad D_5\delta\sigma_5 + D_6\delta\sigma_6 > 0, \end{cases}$$

where η is a normalized vertical profile that peaks in the middle to upper troposphere, r is the relative humidity (=.75), L is the latent heat of condensation, $q_{\text{sat}}(T)$ is the saturation specific humidity at temperature T, D_l is the divergence at level l, $\delta\sigma_l$ is the sigma thickness of layer l, C_p is the specific heat at constant pressure, and m is a "moisture availability factor" that LP introduce to account for the ratio of the total amount of moisture convergence available for condensation to the total amount of moisture convergence below 800 mb and is taken to be 0.8. All parameters are the same as in LP.

Differences with LP are that their model had five equal spaced vertical layers, whereas we have two layers below 800 mb, and we use 12 days for the Rayleigh friction and Newtonian cooling, whereas they use five days. Also, LP impose a geographically fixed wavenumber one variation of the lowest model layer temperature. Instead, as described above, we use the SST field in Fig. 2 after reduction by a uniform 3°C and an exchange coefficient of 0.0006 to force the lowest-level temperature towards the surface temperature. The surface heat flux assumed a constant wind speed of 4 m s^{-1}. The lower levels of dissipation used here were necessary to create a propagating mode that did not disintegrate into small-scale noise too rapidly. To conform with LP, only Newtonian cooling is used in this experiment with no additional imposed cooling profile.

Figure 3 presents a longitude time section of the convective heating at 500 mb on the equator. The model run is begun with an imposed heating centered at 100°E (also the location of maximum SST) that is held fixed for five days. After that, the model determines its own heating according to the convergence-dependent parameterization, the surface heat flux, and the Newtonian cooling. The length of the run is 101 days. The essential features of the results are as follows. A propagating deep convective mode moves east from the heat

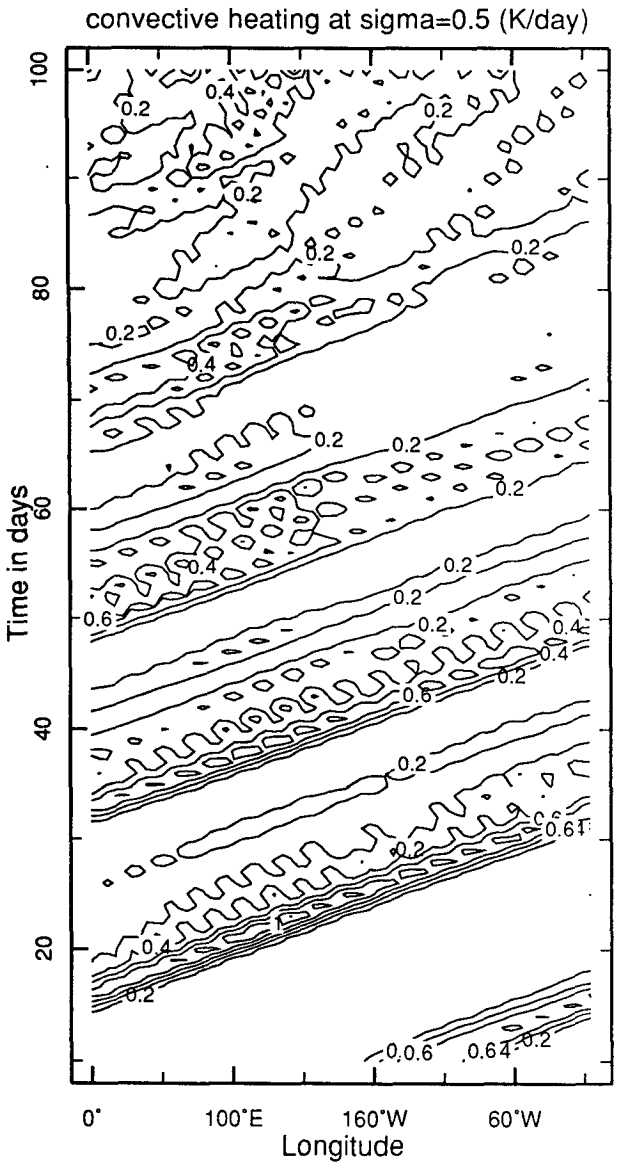

FIG. 3. The convective heating at $\sigma = 0.5$ using the Lau and Peng (1987) convergence-dependent heating formulation in units of kelvin per day.

source located at 100°E and then completes several circuits around the globe. It is generally weaker over the colder water but then strengthens as it returns over the warmer areas. The periodicity is given by the time it takes the disturbance to propagate around the world and is about 17 days. Toward the end of the run the mode weakens and degenerates into small-scale noise. A comparable figure for vertical velocity or divergence is not shown, but given the formulation of the heating these must, and do, correspond almost exactly except for the convergence maximizing to the east of the heating as discussed above. In the first half of the run, the eastward propagating mode is seen to continually emit westward propagating modes as is seen, for example, in Lau et al. (1989).

There are some similarities and some differences between these results and the observations presented in the previous section. First, the existence of a mode that is convecting for the entire duration of its circumnavigation of the globe is clearly in contrast to the observations. Second, the correspondence of the phase speeds of the convection with that of the vertical velocity is also in contrast to the observations. The geographically fixed convection is hardly present here. However, the location of the strongest convection over the warm pool is in agreement with observations. The strengthening of the propagating mode as it moves into that area does agree with WK's hypothesis, at least in principle. However, WK traced this modulation to propagation into the area of an upper-level divergence anomaly rather than a convecting mode. Also, the periodicity derived here is far shorter than that of either the individual convective elements or the slowly moving convective envelopes identified by WK. Further, the dominance of a propagating wavenumber one convective disturbance in the simulation is at odds with WK's results (Fig. 1a). WK did, however, find a single propagating disturbance in the velocity potential anomaly (Fig. 1b). To summarize, the results exhibit too close a tie between convection and convergence and tend to self-organize into a single propagating disturbance, whereas the observations show a more complex longitudinal structure. By tuning the parameters involved, it is possible to produce exponentially growing or decaying solutions. For the more realistic SST shown in Fig. 2, only very high damping prevents exponential growth. This seems to partly result from linearization around a tropical mean basic state. Linearizing around a cooler basic state makes it a little harder to create exponentially growing modes. We consider all these caveats to indicate the drawbacks of the scheme and the lack of robustness of the model oscillation.

b. Betts–Miller convection scheme

1) PROPAGATING DEEP CONVECTIVE MODES

Here we present results using the full Betts–Miller convection scheme and the SST distribution in Fig. 2. For this case we also solve for humidity and introduce surface evaporation. The surface evaporation is computed with the bulk formula as described in section 2a. Zonal mean surface easterlies are assumed only for the purposes of calculating surface fluxes. This parameterization has the effect of enhancing evaporation in regions where the model produces surface easterlies that increase the total wind speed and of suppressing evaporation in regions of surface westerlies where the total wind speed is reduced. The Rayleigh friction and

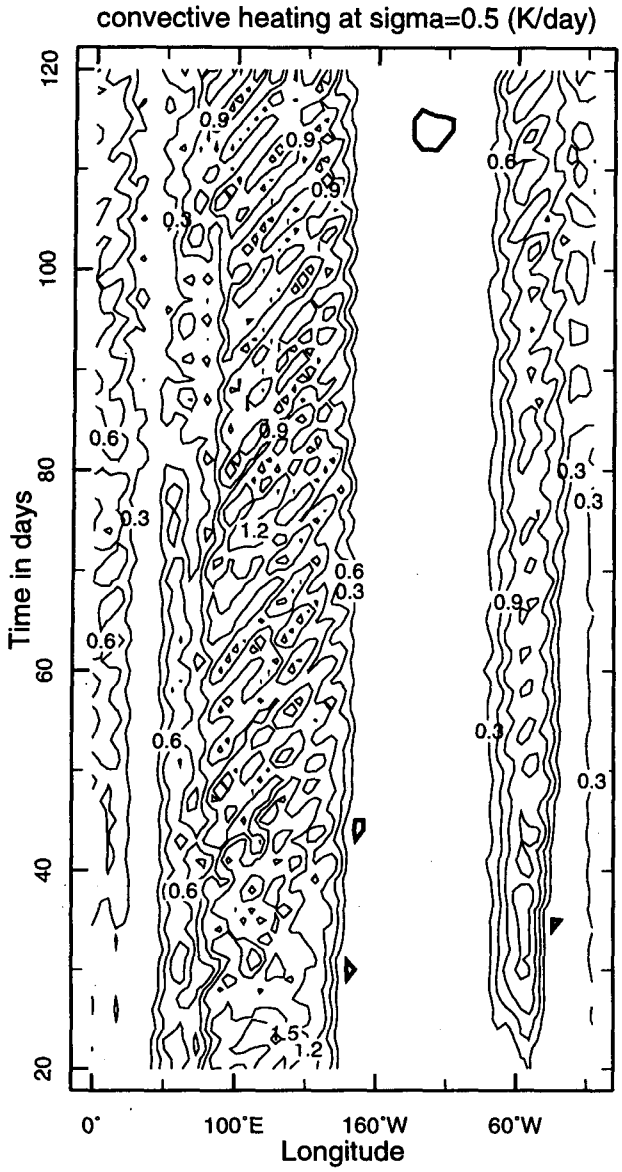

FIG. 4. The convective heating at $\sigma = 0.5$ using the Betts–Miller convection scheme, an exchange coefficient of 0.0004 and minimum wind speed of 3.5 m s^{-1} in the flux computation, and with both moisture convergence and evaporation–wind feedback in the humidity equation.

Newtonian cooling have decay times of 10 days and the boundary layer Rayleigh friction has a decay time of 1.25 days. The additional radiative cooling profile mentioned in section 2a is also imposed.

Figure 4 shows the convective heating at 500 mb on the equator as a function of time and longitude for 100 days of a 121-day run. The data has been smoothed with a 1–2–1 filter in time and longitude. The convection is seen to be geographically rooted over the warm pool centered at 100°E and over the smaller warm regions at 60°W and 0°. In addition, eastward propagating disturbances are seen that move east from the warm pool before dying out close to 180°. The two other warm regions also have less well-defined eastward propagating disturbances that move with the same phase speed. The time period for one of these disturbances to make it around the globe is about 55 days, in reasonable agreement with the speed of the individual convective disturbances identified by WK. What is strikingly absent from the model results, though, is any 30–60-day modulation of convection over the warm pool region.

Figure 5 presents a corresponding Hovmöller diagram of the vertical velocity at 500 mb. Over the warm

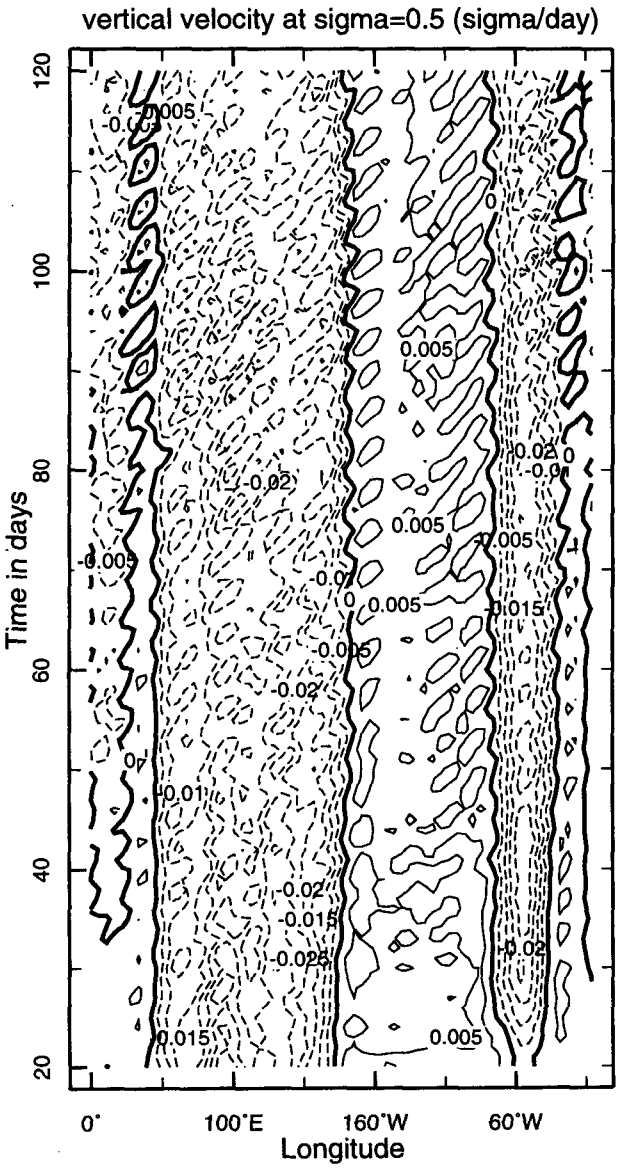

FIG. 5. The vertical velocity at $\sigma = 0.5$ for the experiment in Fig. 4.

pool region, we see slow eastward propagation that is clearly related to the propagation of convective disturbances. Occasionally a rapid eastward propagation over nonconvecting regions is seen, for example, at around day 66. The period of these fast waves is about 15 days, which corresponds closely to, but is a little slower than, the period of the second internal dry atmospheric Kelvin wave. However, even when they occur, they have little influence on convection downstream and are not able to produce the 30–60-day pulsation in the warm pool region that WK hypothesized they could on the basis of observations. We will return to this issue, but for now we will note that this could in part be related to the other obvious model deficiency, that is, the tendency for the convection to be too little concentrated in the first two or three zonal wavenumbers.

The model is clearly capable of producing eastward propagating convective disturbances. There are two possible mechanisms existing in the model that can produce eastward propagation. The first is a convergence mechanism in which low-level convergence maximizes to the east of the center of convection and "triggers" convection, thus moving the center eastward. The second is the evaporation–wind feedback mechanism in which low-level easterlies to the east of the center of convection enhance the local wind speed and increase surface fluxes of heat and moisture. The enhanced fluxes increase the boundary-layer moist entropy and induce convective instability moving the center of convection eastward. It is of importance to know the relative degree to which these mechanisms contribute to the model's behavior.

Figure 6 presents a Hovmöller diagram of the 500-mb convective heating for an experiment in which the convergence of moisture has been artificially set to zero. In this case the humidity is determined solely by surface and convective fluxes and the weak diffusion. For the first 90 days of this run almost no deep convection occurred, but then it establishes itself. Results are shown for days 100 to 200. Eastward propagating modes are again present although they have only half the amplitude of those in the experiment with moisture convergence as well. Their period is however about the same.

Figure 7 presents a Hovmöller diagram of the convective heating for an experiment in which the evaporation–wind feedback was eliminated. In this case the surface fluxes are computed assuming a constant wind speed of 4 m s^{-1}. Eastward propagating disturbances persist with a period also between 55 and 60 days, but they now have the same amplitude as the modes obtained with the complete moisture equation. These modes must be forced by convergence of moisture. What is surprising about this result is that even with a convection scheme that maintains the atmosphere close to neutral stability, and hence in a state with only small CISK, moisture convergence–dependent eastward propagating convective modes can still appear.

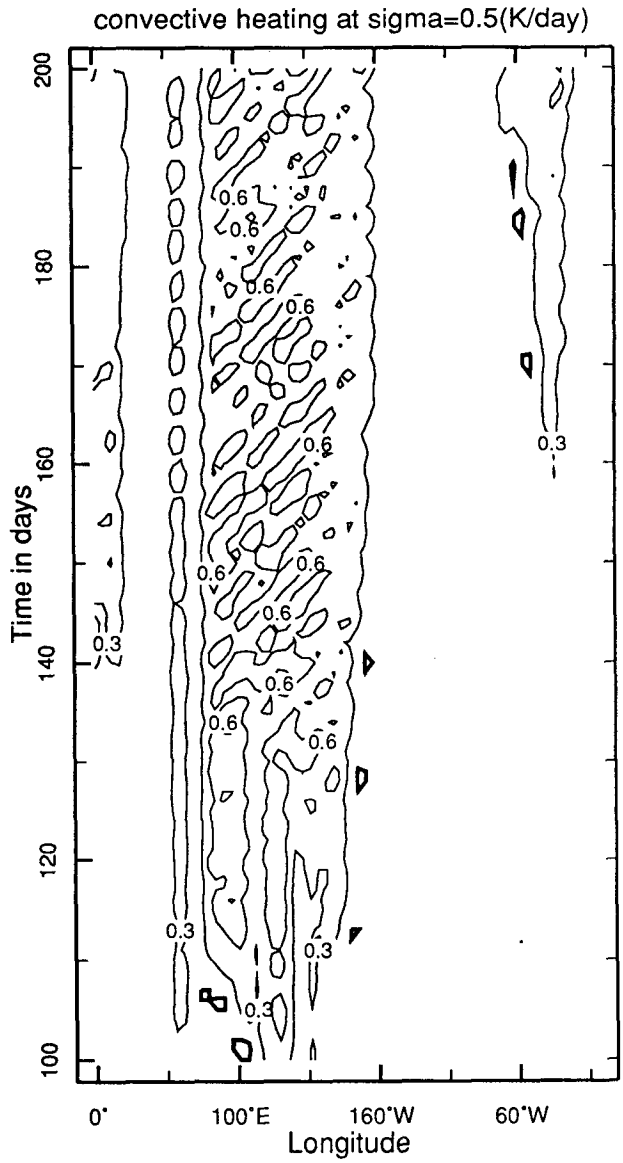

FIG. 6. As in Fig. 4 but for case with moisture convergence excluded from the humidity equation and for days 100 to 200 of the simulation.

It is possible that the dominance of moisture convergence effects over the evaporation–wind feedback is a result of the parameter regime we have chosen. To explore this, we attempted to enhance the role of surface fluxes by increasing the exchange coefficient to 0.0008. We also reduced the minimum wind speed in the bulk formula to 2 m s^{-1} in order to enhance the effects of the wind direction. The convective heating at 500 mb for this case is shown in Fig. 8, and the corresponding 500-mb vertical velocity is shown in Fig. 9. Eastward propagating disturbances are generated that would circle the globe in about 57 days, but as before, convection is suppressed over the colder water.

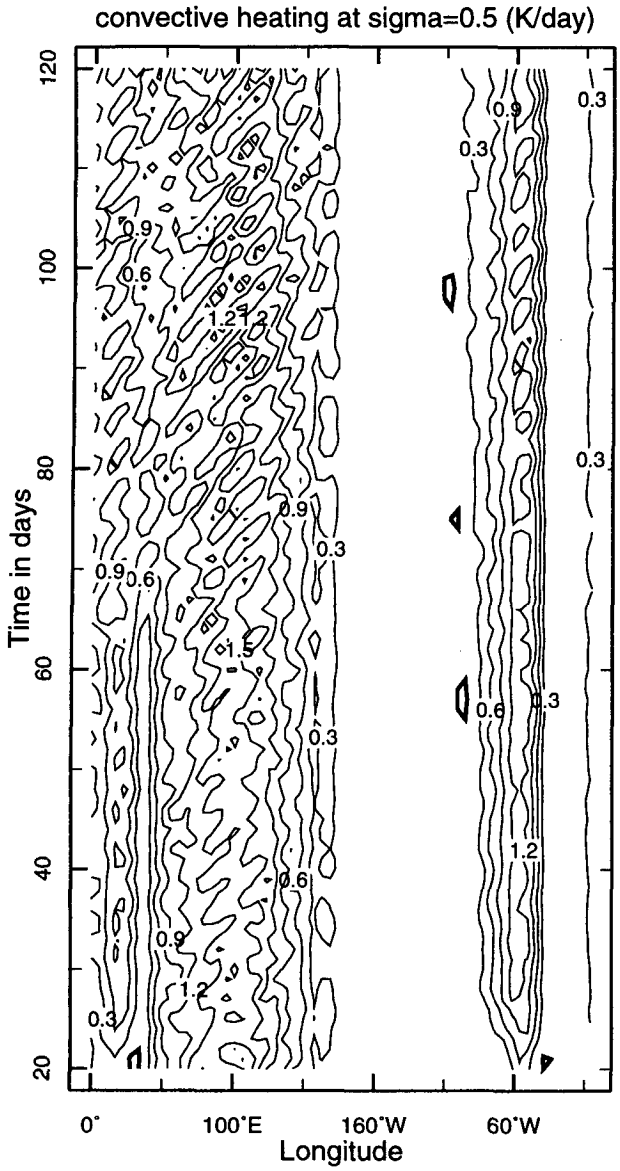

FIG. 7. As in Fig. 4 but for the case with evaporation–wind feedback excluded from the humidity equation.

The evaporation–wind feedback–only case (no moisture convergence) shows a weak eastward propagation with a shorter period of a little under 50 days (Fig. 10) although the stationary component of convection is dominant. Toward the end of the run, more prominent propagation returns but the amplitude is still weak. Rather surprisingly, for the moisture convergence–only case, shown in Fig. 11, no eastward propagation is apparent. In this case the greater surface fluxes prevent an inversion from ever forming over the warm pool and instead cause ubiquitous convection there. It is clear that in this parameter range, the evaporation–wind feedback initiates propagation, but since the propagation is more evident with the complete moisture equation, that moisture convergence can then amplify and organize the disturbances. It is difficult to say which parameter range, this one or the one in the previous experiments, is more realistic. The longer periodicity when the full moisture equation is used appears to be consistent with the GCM results of Neelin et al. (1987), who found generally longer-period modes when the wind speed dependence of evaporation was shut off in the GFDL GCM. This suggests that the

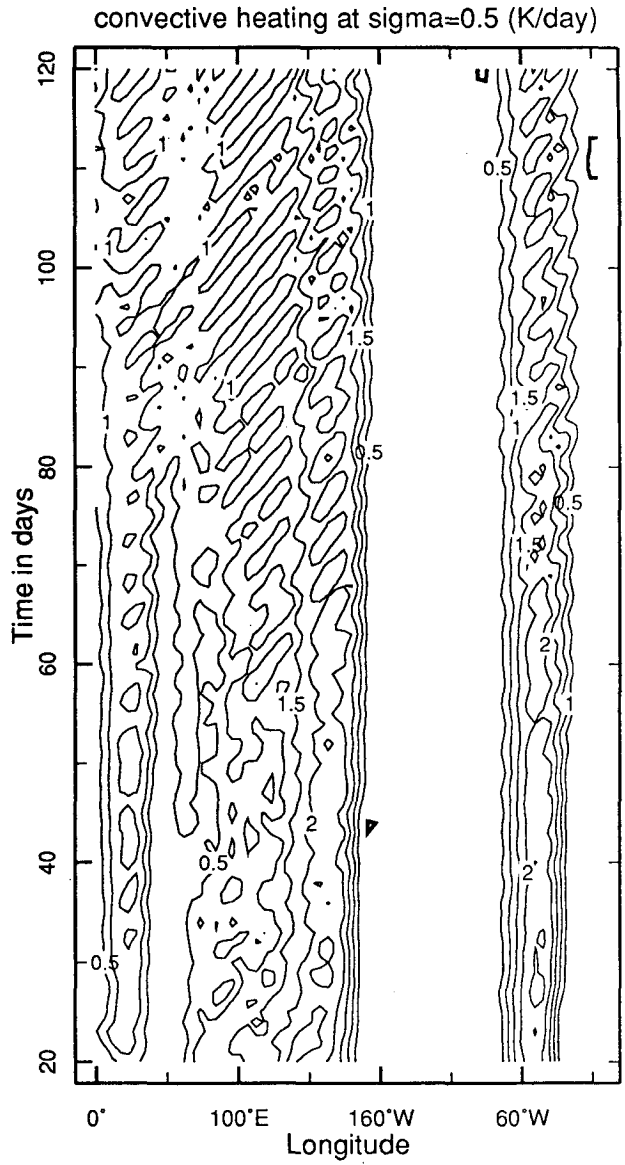

FIG. 8. The convective heating at $\sigma = 0.5$ using the Betts–Miller convection scheme, an exchange coefficient of 0.0008 and minimum wind speed of 2.0 m s^{-1} in the flux computation, and with both moisture convergence and evaporation–wind feedback in the humidity equation.

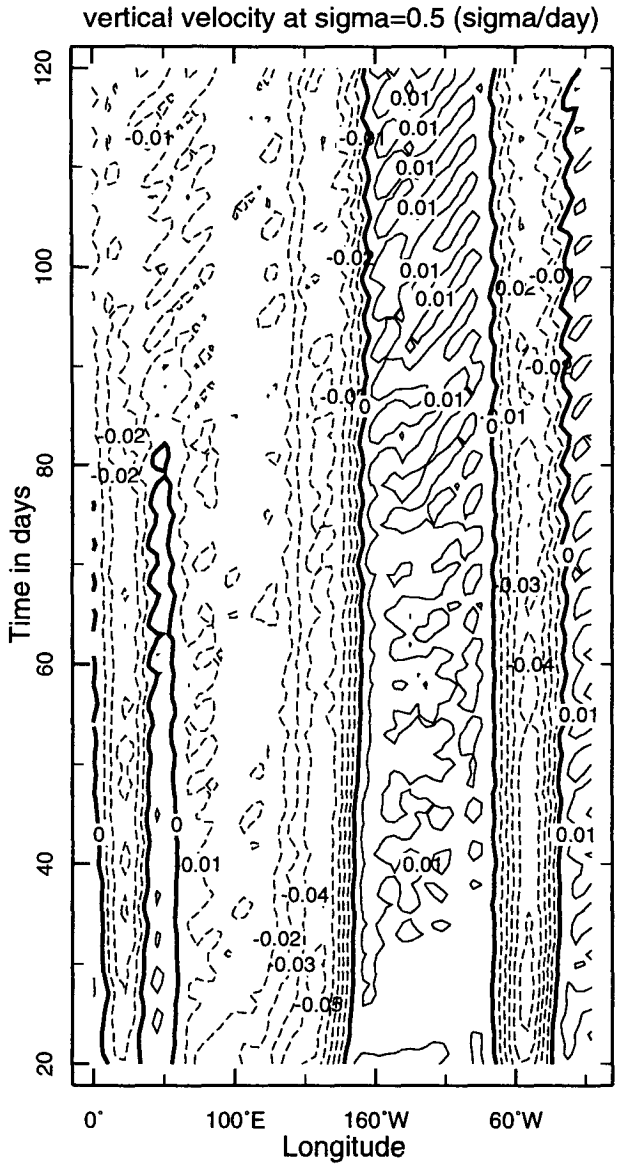

FIG. 9. The vertical velocity at $\sigma = 0.5$ for the experiment in Fig. 8.

evaporation–wind feedback acts to speed up the modes.

The mechanism for eastward propagation of the convergence mode is easily seen in the model. Figures 12, 13, and 14 present longitude height cross sections for the region 80°E to 150°W of the model divergence, equivalent potential temperature, and convective heating, for three successive days in the model run with both moisture convergence and evaporation–wind feedback, an exchange coefficient of 0.0004, and minimum wind speed in the surface flux calculation of 3.5 m s^{-1}. The equivalent potential temperature figures show the actual equivalent potential temperature for the lowest level ($\sigma = 0.95$) and the saturation values for the layers above. Hence, stability can be assessed directly by comparing the value shown at the lowest level with those above. We will refer to the two different quantities by the single symbol θ_e in the discussion that follows. It can be seen from these figures that a low-level θ_e inversion is present wherever there is no convective heating. It is also very apparent that the divergence field forced by the convective heating has a pronounced westward tilt with height, which has been pointed out, in data and in models, by previous authors (e.g., Hartmann et al. 1984). This phase tilt has the effect of placing the lowest-level convergence eastward

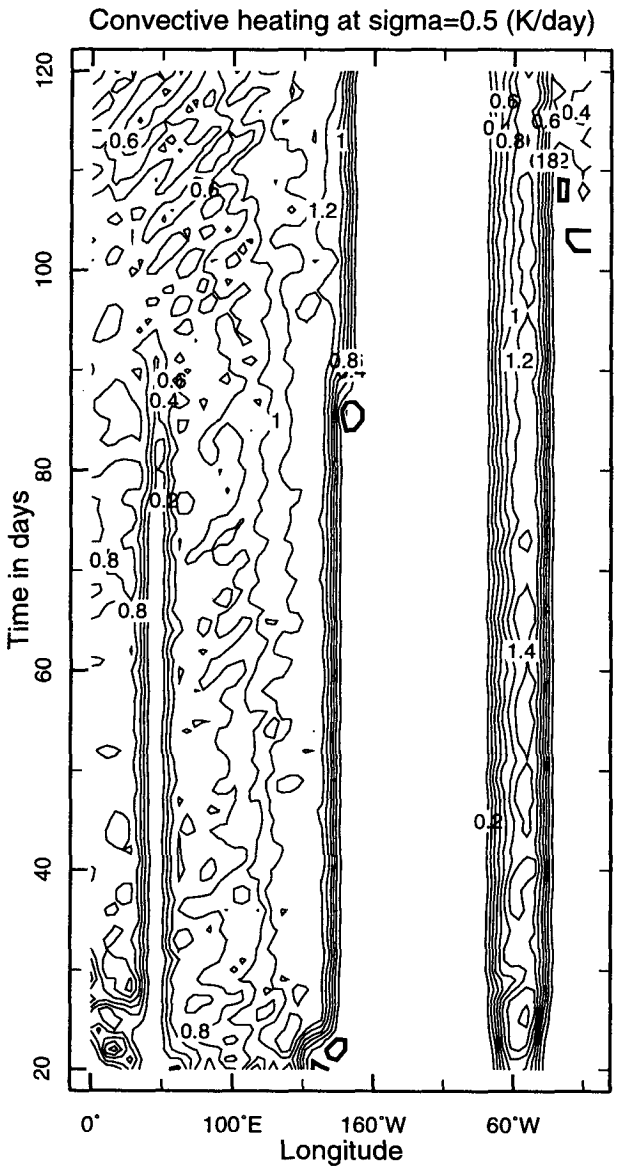

FIG. 10. As in Fig. 8 but for the case with moisture convergence excluded from the humidity equation.

of the convective heating maximum. For example, on day 81 (Fig. 12) the convecting regions at 120°E and 140°E induce surface convergence to their east and out to 160°E. A disturbance farther west has induced convergence at 105°E. The induced surface convergence is often placed under a θ_e inversion, as is the case at 105°E and 130°E. On the next day (Fig. 13), we see that the surface convergence has eroded these inversions and convecting disturbances have propagated into these areas. On this day we again see the systematic shift of the surface convergence east of the convective heating, and this continues to erode the inversions now at 110°E and 135°E such that on day 83 (Fig. 14) convection has been initiated in these areas.

It can be seen in these figures that an inversion persists east of 160°W. Deep convection never propagates east of this longitude. However, between this longitude and the next patch of warm water, shallow convection persistently occurs. Shallow convection cools and moistens at cloud top due to evaporation of cloud drops and warms and dries below (Betts 1986; Albrecht et al. 1979; Soong and Ogura 1980). This maintains the low-level inversion while preventing the low-level θ_E from increasing due to the surface fluxes of heat and moisture. Hence, shallow convection, in this model, releases conditional instability created by the combined effects of radiative cooling and surface fluxes while working to prevent deep convection from occurring. Kloesel and Albrecht (1989) and Firestone and Albrecht (1986) have also suggested, on the basis of observations, that this process is responsible for the regulation of convection over the equatorial Pacific.

2) MODEL CLIMATOLOGY

The climatology for this run is also of interest. Model representations of the intertropical convergence zone (ITCZ) have recently come under scrutiny. In the real atmosphere there is typically one off-equatorial ITCZ, although at times there can appear to be two ITCZs straddling the equator in the west Pacific (e.g., Fu et al. 1990). Holton et al. (1971) claimed that wave–CISK causes the ITCZ to be off the equator, since moisture convergence maximizes in off-equatorial Rossby–gravity waves where the frequency of the wave equals the local Coriolis frequency. Hess et al. (1993) found that in a GCM with a zonally symmetric SST twin off-equatorial ITCZs were found when a convergence-dependent Kuo convection scheme was used, but that one ITCZ located on the equator and over the maximum SST was formed when moist convective adjustment was used. They attributed the twin ITCZs to the organization of convection by Rossby–gravity waves with maximum convergence off the equator. In three other experiments with SST symmetric about the equator, Swinbank et al. (1988) and Hayashi and Sumi (1986), using convergence-dependent convection schemes, found twin ITCZs, whereas Lau et al. (1988), using MCA, found a single ITCZ on the equator.

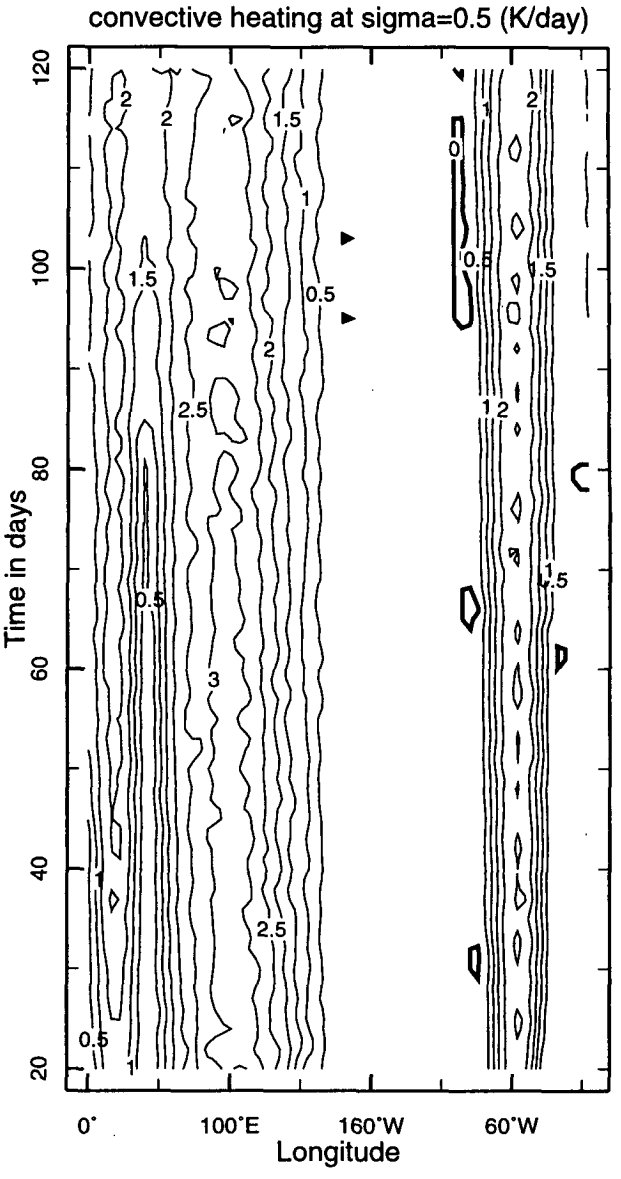

FIG. 11. As in Fig. 8 but for the case with evaporation–wind feedback excluded from the humidity equation.

Figure 15 shows the lowest-level convergence, the zonally averaged vertical velocity, and equatorial cross sections of the vertical velocity and drying by convection, averaged over the last 60 days of the run with the complete moisture equation, an exchange coefficient of 0.0004, and minimum wind speed in the surface flux calculation of 3.5 m s^{-1}. The model is seen to produce a single ITCZ centered on the equator but with a tendency to maximize convergence off the equator in the warm water regions. The equatorial cross section of vertical velocity reveals that the model produces the characteristic baroclinic structure of tropical flow. The cross section of convective drying is presented to show

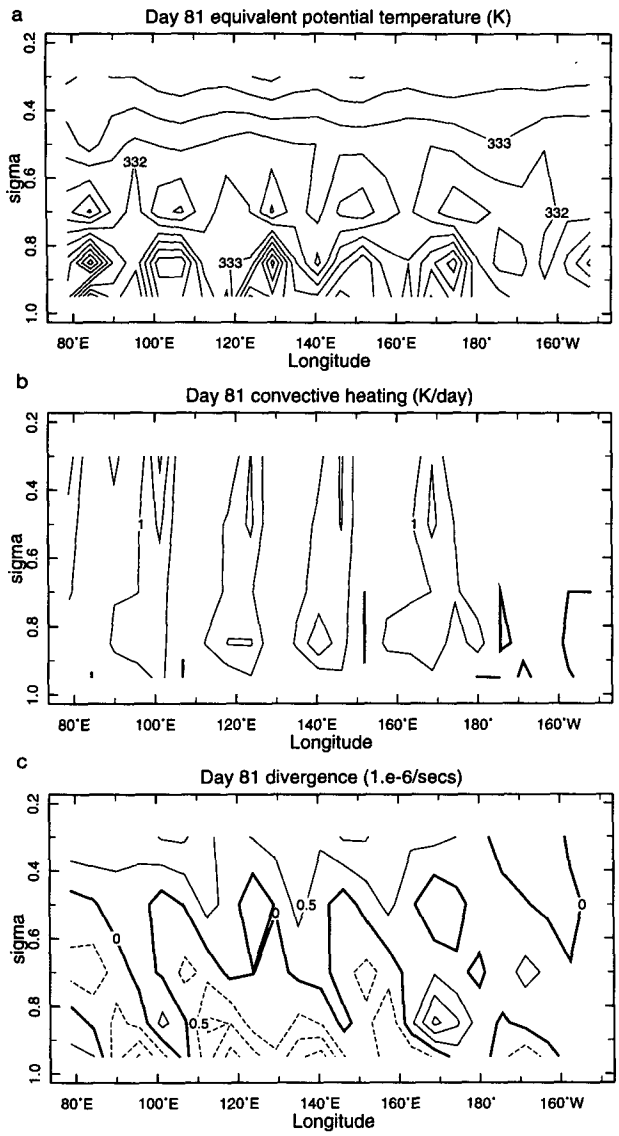

FIG. 12. Longitude–height cross sections on the equator of (a) the divergence (10^{-6} s^{-1}), (b) equivalent potential temperature (K), and (c) the convective heating (K day^{-1}) for day 81 of the experiment shown in Fig. 4.

the important role that shallow convection plays in the region between 160°W and 90°W. In this region shallow convection is seen to moisten at around 850 mb and dry the near-surface air. The same process cools at 850 mb and warms the air below. The combined effect is to allow the surface flux to be balanced while maintaining an inversion that inhibits deep convection. The existence of the inversion, both in the nonconvecting regions and intermittently in the convecting regions, was found to depend on the imposed radiative cooling profile. The maximization of cooling near the surface acts to suppress instability to deep convection. If there were no near-surface radiative cooling the surface flux would have to be balanced by convective cooling. This would necessitate deep convection, since shallow convection actually warms the lowest layer. Thus, low-level radiative cooling is necessary for the development of shallow convection and plays an important role in the regulation of convection.

5. Discussion and conclusions

We have presented a case study of the interaction between convection and dynamics in a new linear primitive equation model with a Betts–Miller convection scheme. The dynamical model has been recently developed as an accurate and efficient climate model. We have sought to develop a model that is general, of arbitrary resolution, and that can be run in linear or non-

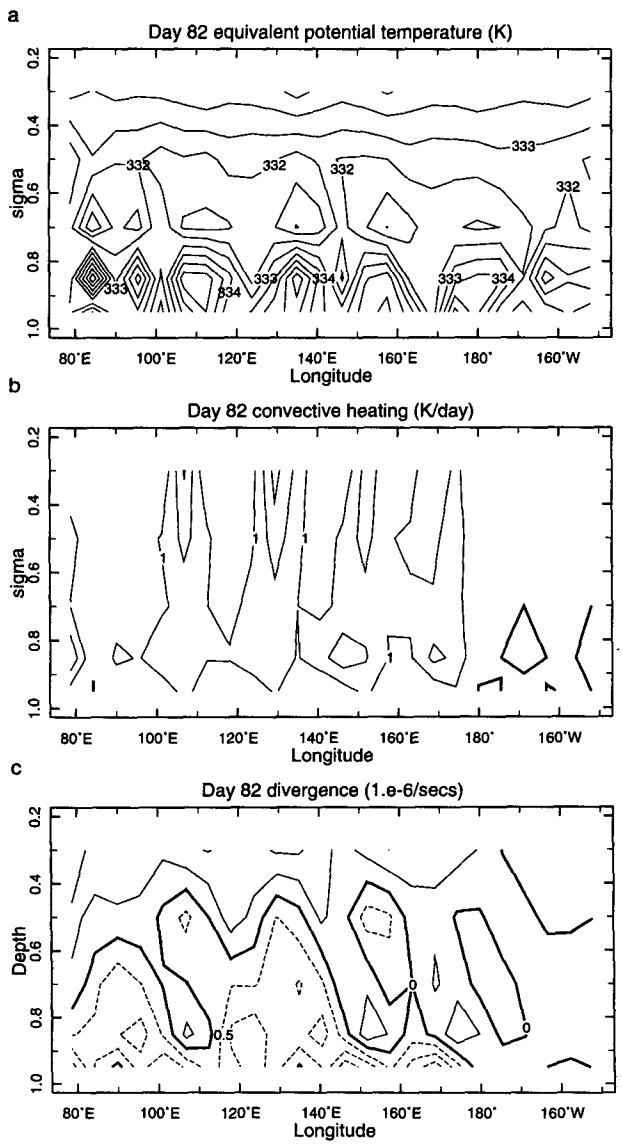

FIG. 13. As in Fig. 12 for day 82.

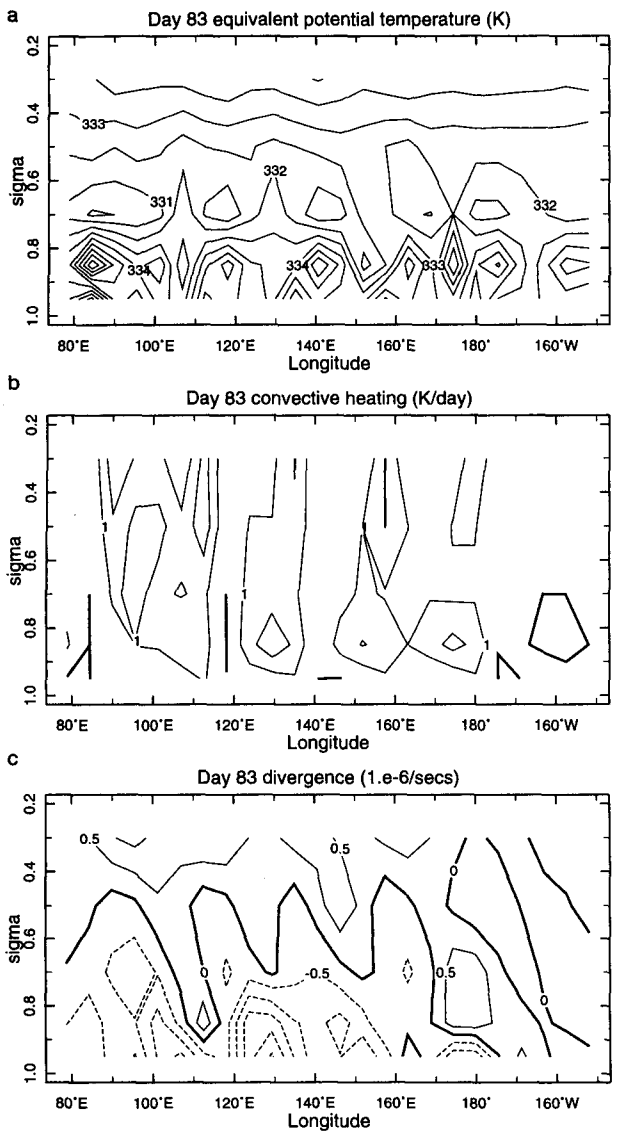

FIG. 14. As in Fig. 12 for day 83.

linear mode, with interchangeable physics packages. We aim to avoid some of the complexity and intractability of GCMs but also to overcome the serious limitations of more simple models such as those of Zebiak (1986), which were enumerated by Seager (1991). A key feature of the current model is the introduction of a new method of solving the primitive equations on a sphere using normal modes that allows stable integration for very long time steps, thus ensuring computational efficiency.

Because of the importance of convection in driving the steady-state thermally direct tropical circulations, and its importance to intraseasonal and interannual variability, we have chosen to first test this model by studying its behavior when coupled with one of a suite of recently developed convection parameterizations. To get an idea of the range of behavior possible in a relatively controlled setting, we have chosen to focus on the intraseasonal oscillation, rather than attempt at this time to reproduce observed climatological flows or interannual variability. This is done by using a water-covered earth with an idealized sea surface temperature distribution. The climatology of this idealized case is also briefly discussed.

As a benchmark calculation we first used a simple heating parameterization in which the convective heating was proportional to the low-level moisture convergence and in which the low-level moisture was tied to the surface saturation value with a fixed relative humidity. This scheme was copied from Lau and Peng (1987). The model was damped with Newtonian cooling and Rayleigh friction. We departed from Lau and Peng by assuming a zonally and meridionally varying SST and by including a surface heat flux. After an initial heating was turned off, the model produced an eastward propagating convective disturbance that circled the globe in less than 20 days. A few circuits were completed before the mode decayed into higher wavenumber propagating modes and a weak steady circulation with heating over the warm SST regions. The propagating mode originates in the maximization of low-level convergence to the east of the heating due to the forced Rossby and Kelvin wave structures. The faster phase speed obtained here relative to Lau and Peng (1987) may be due to the absence of numerical damping that, in their model, is introduced by the semi-implicit time integration. We found that by altering the SST field and changing various parameters, it is quite easy to get propagating disturbances that favor small wavenumbers and are near neutral in that they persist for more than 100 days. It is equally easy to suppress these modes by other alterations.

In a review of the unfiltered observational data, it was noted that the single propagating disturbance common in wave–CISK studies that remains coherent around the globe was different to the observed phenomenon. The observed convection exhibits a strong geographically fixed component together with a slow eastward propagation of convective disturbances that die out over the central Pacific. It is possible that the disturbances excite dry atmospheric waves that then encircle the globe rapidly (about 15-day period) and can initiate a subsequent slowly eastward propagating convective disturbance over the east Indian Ocean. The 30–60-day period is then set by two different phenomena propagating at two different speeds in different parts of the equatorial band. No wave–CISK theory reproduces this aspect of the phenomenon.

Introduction of the Betts and Miller (1986) convection scheme radically changed the simulation. The scheme works on buoyancy considerations alone and does not depend on moisture convergence. Nonetheless, eastward propagating disturbances were created

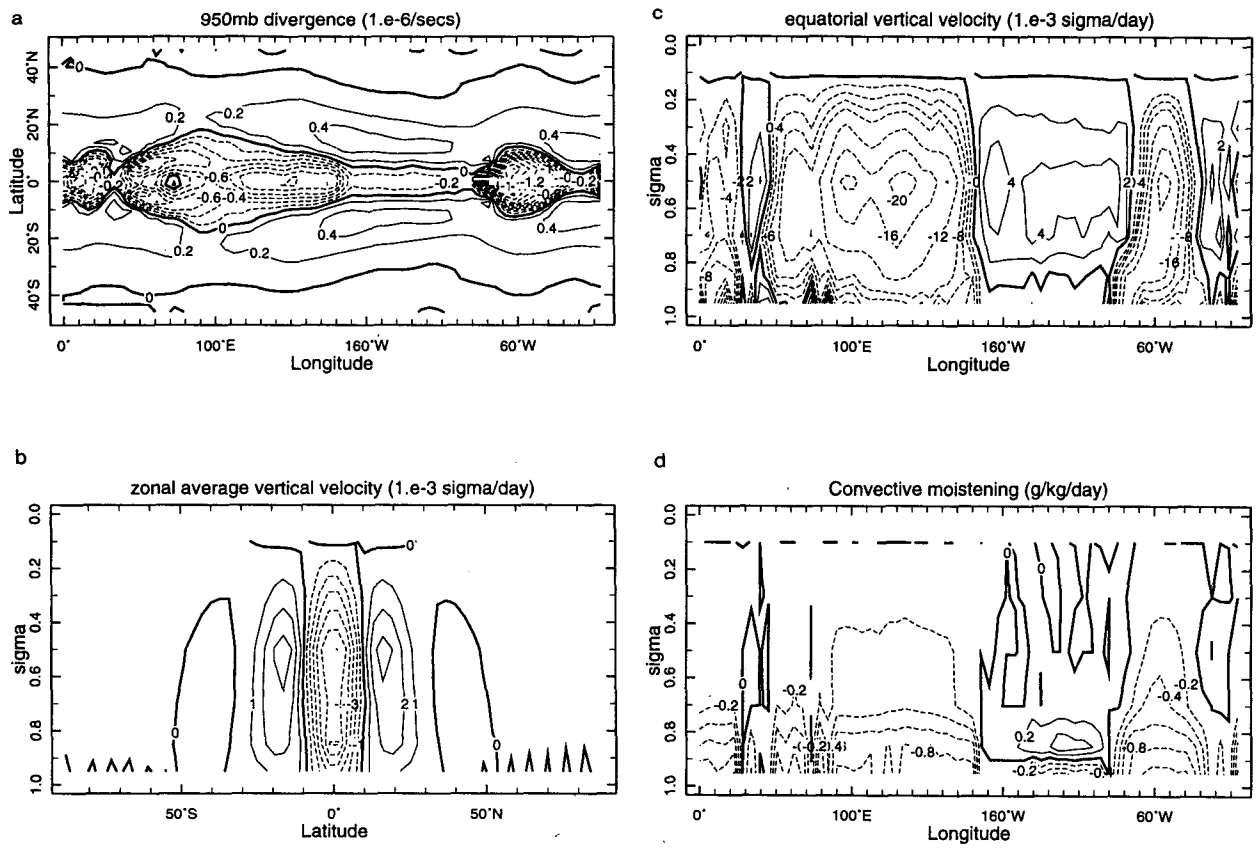

FIG. 15. Averages over days 40 to 100 of the experiment shown in Fig. 4 of (a) the 950-mb divergence (10^{-6} s^{-1}), (b) the zonally averaged vertical velocity (10^{-3} σ/day), (c) the vertical velocity (10^{-3} σ/day) on the equator, and (d) moistening by convection (g kg^{-1}/day) on the equator.

and persisted throughout the model run and would apparently persist indefinitely. A single disturbance would propagate around the world in about 54 days. However, this does not occur, but instead disturbances originate in, and propagate east from, a region of persistent convection over the warmest water region and die out over colder waters to the east. While these features of the simulation are much more realistic than in the simple convergence-dependent heating case, no 30–60-day pulsation of convection occurs over the warmest water region as is observed. This is attributable to the most significant departure of the model from reality: the model favors a wavenumber three or higher distribution of propagating features. In contrast, observations show convective clusters of rather indistinct wavenumber over the warm pool and fast wavenumber one modes in the velocity potential field that connect the warm pool clusters. Whatever in nature acts to organize the propagating disturbances into large-scale features is clearly absent in this model.

We found an important role for the low-level inversion in regulating tropical convection. An inversion is present in the model wherever no deep convection is occurring. The inversion creates a stable layer in the lower troposphere that prevents deep convection until either surface fluxes or low-level convergence can increase the lowest-level θ_E so it is greater than the θ_{ES} above. In the warmest water regions this occurs relatively easily. Over colder waters subsidence warms and dries the air above the inversion, which, combined with the lower near-surface θ_E, means that the column never becomes unstable to deep convection. Instead, shallow convection occurs that, together with radiation, balances the tendency of the surface fluxes to increase the low-level θ_E while also maintaining the inversion. Although we expect that a similar process occurs in other models that contain shallow convection parameterizations (e.g., the model of Slingo et al. 1993), few model studies have drawn attention to this important aspect of the tropical circulation. These results are a model verification of the observations on the role of the inversion in regulating convection presented by Firestone and Albrecht (1986) and Kloesel and Albrecht (1989).

The eastward propagating modes found with the Betts–Miller convection scheme are affected by both evaporation–wind feedback and low-level convergence of moisture. If the evaporation–wind feedback is removed, then a moisture-convergent mode is seen

with a single disturbance that would encircle the globe in about 60 days. Although the phase speed in this experiment is slower, this simulation is very similar to the complete model and also contains no evidence of a 30–60-day pulsation of convection over the warm pool region. If the effect of moisture convergence is suppressed, then almost all deep convection and propagation is suppressed. The last result raised the issue of whether this result is forced by the parameter range we chose. If the surface fluxes are increased, then eastward propagating modes remained. These were still influenced by the effects of moisture convergence but weak eastward propagation remained in a case with the evaporation–wind feedback only. Because of the uncertainty involved in modeling surface fluxes in the absence of a reliable boundary-layer model, we cannot determine which parameter setting is more correct. Hence, although moisture convergence is dominant in the experiments we have presented, the role of the evaporation–wind feedback cannot by any means be excluded. This is a matter we intend to investigate further.

Although we have clearly indicated a connection between convection and low-level moisture convergence, the mechanism is different from that in most simple wave–CISK models of the intraseasonal oscillation, including that presented in section 4a. In this model low-level mass and moisture convergence to the east of convective heating centers increases the low-level θ_E such that the θ_E inversion that prevails in the absence of convection is eroded, allowing convection to occur. In contrast, many wave–CISK models assume the low-level θ_E is constant, but since the convective heating is proportional to the low-level moisture convergence, enhanced convection can occur in the absence of changes in low-level θ_E. This was the case in the model in section 4a.

The difference lies in the assumption in wave–CISK studies that the atmosphere is conditionally unstable everywhere. In that case moisture convergence triggers convection that will lead to an extraction of CAPE by the flow. This can also occur in models that enforce necessary conditions, such as on moisture convergence or relative humidity, that artificially suppress convection even when the column is unstable, thus allowing a buildup of CISK and CAPE. In this model the atmosphere is either slightly unstable to moist ascent or stable. If the atmosphere was neutral to moist ascent and the low-level θ_E was held fixed, then any amount of moisture convergence would not alter the atmospheric thermodynamic structure. This is because the adiabatic cooling (moisture convergence) will balance exactly convective heating (drying). Or alternatively, a neutral atmosphere has no CAPE available for extraction by the flow. The convergence of moisture at uniform θ_E that caused propagation in the wave–CISK model for this reason cannot cause propagation in the model with the Betts–Miller scheme.

The moisture convergence mode in this model works differently from that in wave–CISK theory. While low-level convergence is maximized to the east of convective heating regions, it occurs in areas where the atmosphere is stable to moist ascent. The moisture convergence acts to increase the low-level θ_E such that the inversion above is eroded and convection can occur. The eastward propagating mode can only exist because of modification of the boundary-layer θ_E by the dynamics.

Despite some similarities to observations numerous differences remain, most notably the absence of the large-scale organization of propagating features seen in the data. The central difference is that in the data, at any one time, there is a single cluster of convection over the warm pool region with possible other clusters over South America and Africa (although there is a tendency for suppression of the former when warm pool convection is active). In contrast, the model produces typically three or so distinct convective centers over the warm pool at any one time. It is also true that over the nonconvecting region the model also produces higher wavenumber disturbances than observed but it is thought that this is a reaction to, rather than a cause of, the incorrect zonal scales in the convecting region. In nature it appears that convection acts to suppress convection in regions around it more than in the model. As argued by Emanuel (1987), this suppression forces disturbances to favor larger zonal scales. What can it be that the model is excluding?

Since many GCM studies of the intraseasonal cycle have used aquaplanet models with no zonally asymmetric forcing, it is difficult to make direct comparisons with the results here. However, Lau and Lau (1986) have presented diagnostics of the oscillation in the GFDL GCM. An empirical orthogonal analysis picked out a dominant wavenumber one mode that propagated eastward with a period of 25–40 days. After compositing on the basis of this EOF analysis and bandpass filtering the model output, they show Hovmöller diagrams of zonal velocity and precipitation. The precipitation within this mode is largely confined to the west Pacific–Indian Ocean region. Over the west Pacific there is a suggestion that the precipitation propagates east slower than the large-scale flow field in which it is embedded. This has some similarities to the observed behavior although the details are very different. Unfortunately, they do not show any Hovmöller diagrams of the unfiltered data, so direct comparison with the observations of WK is not possible and it may, in fact, be the case that the EOF analysis is unduly emphasizing the largest zonal scales.

Although the GCM is fully nonlinear, it is doubtful this is the cause. Almost all existing theories of the oscillation rest on interactions between thermodynamics and linear waves. No doubt nonlinearities modify the oscillations, but they are unlikely to be responsible for setting the horizontal scale. The GFDL GCM em-

ploys a moist convective adjustment scheme, which imposes the requirement that relative humidity exceed a certain value before convection occurs. It might be thought that this will assist in forcing a large zonal scale response by suppressing convection in drier regions. However, imposing such a condition in this model left the basic character of the propagating disturbances in the model unchanged and did not alter the preferred zonal wavenumber.

The cause of the lack of mesoscale organization in the model must lie in either the model's dynamics or thermodynamics. For example, it could be a result of inadequate treatment of the subtle interactions between convective, radiative, and surface fluxes in the boundary layer. We have shown that the one thing in the model that suppresses convection is the presence of a low-level inversion that provides a stable layer through which low-level air cannot penetrate. Although this inversion is present in the model, it appears that in warm water regions it is quite easily destroyed by fluxes and moisture convergence. If it were more robust, it might act to suppress convection more extensively than it does now. Soong and Ogura (1980) showed how an inversion could be created from a stable profile through mixing and then be intensified by shallow convection. In equilibrium subsidence warming and drying balance the radiative cooling and convective cooling and drying at cloud top (Betts and Ridgeway 1988). While a process similar to this clearly occurs in the model, the details of this interaction are not correct. For example, the subsidence does not peak within the inversion as observed but in the midtroposphere. However, Soong and Ogura found that sizable low-level subsidence was absolutely essential to the development of a strong inversion.

This line of reasoning, and the results we have presented, suggest a number of improvements that can be made to deal with these deficiencies. The importance of the radiatively induced subsidence to the initiation and maintenance of the inversion suggests that an improved treatment of radiation is essential. Radiative cooling drives a subsidence allowing adiabatic warming due to compression to balance the cooling. Ascent of air in convecting regions is necessary for conservation of mass. The two regions are connected via surface fluxes, which ultimately have to balance both convective drying and radiative cooling (Sarachik 1978). In this interaction radiation is the progenitor and the rest is response. It is not to be expected that a realistic representation of the tropical atmosphere can be had without adequate treatment of radiation. For example, the simplistic treatment of radiation in this model will necessarily cause an incorrect background subsidence. Incorrect subsidence will affect boundary-layer moisture through a poor representation of subsidence drying. That in turn will have an impact on the frequency and intensity of convection.

Equally important is an improved treatment of boundary-layer processes and the surface fluxes. Since the shallow convection simulates the effects of convection and mixing in the cloudy portion of the boundary layer, the main focus must be on the subcloud and surface layers and on the momentum mixing throughout the entire layer. Incorporation of a boundary-layer model would overcome the present unsatisfactory situation of having to calculate fluxes with values appropriate to the 950-mb level, rather than the surface layer, and the resulting uncertainty in the proper value to use for the exchange coefficient. A surface flux scheme must also include a more reliable treatment of the fluxes in low wind speed conditions than we use here. Miller et al. (1992) demonstrated a very high degree of sensitivity of the ECMWF model, including in its tropical intraseasonal variability, to the details of this parameterization.

While these changes to the treatment of thermodynamic processes will certainly improve the model's realism, it is not immediately apparent that they will lead to a more spatially organized simulation of the convective anomalies associated with intraseasonal oscillations. Model dynamics may also be at fault. Yano and Emanuel (1991) have argued that vertical propagation of Kelvin waves acts as a scale selection mechanism. This is because waves with small horizontal scales are strongly damped by upward propagation into the stratosphere. In the real world this preferential loss of energy from the troposphere will cause a planetary-scale bias in the convectively forced circulations. This scale selection process cannot happen in our model because, in common with all operational global models, the top boundary condition of no vertical velocity prevents energy loss to space. However, GCMs often include some damping in high layers to prevent reflections of energy by the model top. This may parameterize the process that Yano and Emanuel suggest. We intend to investigate this in the near future.

The likelihood that there will be no quick fixes for the convective-scale selection problem is illustrated by the experience of Slingo et al. (1993). They used a model based on the ECMWF model. As well as the Betts–Miller convection scheme, their model included representations of surface fluxes, boundary-layer processes, and radiation that are, arguably, state of the art. Nonetheless, their model has the same tendency to create three or four convective disturbances over the warm pool region as found in our model. Their results also show no evidence of any larger-scale organization of convection into convective envelopes. In the Slingo et al. model the convection was, if anything, less organized when the Kuo scheme was used. It appears that their model, and ours, conform to the claim made by Weickmann and Khalsa (1990, p. 977) that "the GCM versions of the oscillation are more reminiscent of the continuous eastward propagating individual elements

sometimes observed within the convective energy envelope."

A single ITCZ over the warmest water formed in the model experiments with the Betts–Miller scheme. This result has been robust over a range of experiments. The only exception has been a weak tendency to form two convergence zones in a run with zonally symmetric SST and a Newtonian cooling to a dry-adiabatic lapse rate. In that run, occasional periods with two ITCZs appeared, but after a day or two they collapsed again into one. Given the lack of convergence dependence in this convection scheme, it is not surprising that it forms one equatorial ITCZ in these idealized experiments. This is consistent with the results of an MCA scheme in the GFDL GCM (Lau et al. 1988). In nature mechanisms other than organization of convection by propagating waves are capable of keeping the ITCZ off the equator and it may be that, given realistic SSTs, this model will be able to reproduce this aspect of the observations. We plan to investigate this shortly.

To conclude, we have demonstrated the existence of an eastward propagating convective mode in a model with a Betts–Miller convection scheme that is created by low-level moisture convergence but may, under certain conditions, also be effected by evaporation–wind feedback. The propagation speed is slow relative to many other models but not in comparison to observations. However, the model disturbances do not organize themselves into large-scale systems capable of suppressing convection around them in the way observed convective clusters do. We have speculated that a greater agreement between model and reality will have to await a more realistic treatment of radiation and boundary-layer processes. To that end, we have developed a modified version of the Ramanthan and Downey (1986) radiative transfer scheme and plan to implement it in the model soon and are experimenting with more detailed boundary-layer schemes. We further plan to examine the behavior of the Betts–Miller convection scheme in studies of other phenomena including the tropical climatology and interannual variability.

Acknowledgments. We wish to thank Mark Cane, Mike Wallace, Ed Sarachik, Yochanan Kushnir, and Roger Daley for valuable discussions relating to this work. RS wishes to thank the Joint Institute for Study of the Atmosphere and Ocean for its support and patience during the model development phase of this work and the NOAA Postdoctoral Program in Climate and Global Change for support during the last stages. SEZ was supported by National Science Foundation Grants ATM89-21804 and ATM92-24915.

APPENDIX

Model Equations

We begin with the primitive equations on a sphere written in sigma coordinates and linearized about a motionless mean state with a basic-state temperature $\bar{T}$ as a function of sigma only. The basic-state temperature was created to be typical of a tropical atmosphere. The equations are discretized on a vertical grid with L layers of thickness $\delta\sigma_l$ and with midpoints at σ_l. Discretization conforms to the energy conserving form as given by Corby et al. (1977) except in the vertical advection of temperature, as will be discussed below. The momentum equations can be written as

$$\frac{\partial \mathbf{u}}{\partial t} - \partial\Omega\mu\mathbf{v} + \frac{1}{a}(1-\mu^2)^{-1/2}\frac{\partial \mathbf{P}}{\partial \varphi} = \mathbf{F}, \quad \text{(A1)}$$

$$\frac{\partial \mathbf{v}}{\partial t} + \partial\Omega\mu\mathbf{u} + \frac{1}{a}(1-\mu^2)^{1/2}\frac{\partial \mathbf{P}}{\partial \mu} = \mathbf{G}, \quad \text{(A2)}$$

where $\mathbf{u}$ and $\mathbf{v}$ are the vectors containing the zonal and meridional velocities of each layer, respectively, $\mu = \sin\theta$, where θ is latitude, a is the radius of the earth, Ω is the rotation of the earth, $\mathbf{F}$ and $\mathbf{G}$ are the zonal and meridional forcings for linear motions and can include nonlinear terms, friction, etc.; $\mathbf{P}$ is given by

$$\mathbf{P} = \mathbf{\Phi} + R\bar{\mathbf{T}}\pi, \quad \text{(A3)}$$

where Φ is the vector containing the layer geopotentials ϕ_l, R is the gas constant, and $\pi = \ln(p_s/\bar{p}_s)$, where p_s is the total surface pressure and $\bar{p}_s$ is the global mean surface pressure. The hydrostatic equation at layer l is written

$$\phi_l = \phi_s + R\left(b_l T_l + \sum_{i=l+1}^{L} a_i T_i\right), \quad \text{(A4)}$$

where ϕ_s is the surface geopotential, assumed zero, and a_l and b_l are coefficients, the exact form of which will be determined later. The temperature at layer l is given by

$$\frac{\partial T_l}{\partial t} + \left[\dot{\sigma}\frac{\delta \bar{T}}{\delta\sigma}\right]_l + \kappa\bar{T}_l \times \left(a_l \sum_{s=1}^{l-1} \delta_s \delta\sigma_s/\delta\sigma_l + b_l\delta_l\delta\sigma_l\right) = \dot{R}_l, \quad \text{(A5)}$$

where $\kappa = R/C_p$, with C_p equal to the heat capacity at constant pressure, and δ_s is equal to the horizontal divergence at level s. Here $\dot{R}$ represents all forcing, including diabatic heating and nonlinear terms, and $\dot{\sigma}$ is the vertical sigma velocity. The last term on the left is the linear part of the energy conversion term, which was written in the energy conserving form given by Corby et al. (1977).

The continuity equation is

$$\frac{\partial \pi}{\partial t} + \delta_l + \frac{\dot{\sigma}_{l+1/2} - \dot{\sigma}_{l-1/2}}{\delta\sigma_l} = N_l. \quad \text{(A6)}$$

In (A6) N_l represents terms that advect mass. The surface pressure equation is given by vertically integrating (A6):

$$\frac{\partial \pi}{\partial t} + \sum_{l=1}^{L} \delta_l \delta\sigma_l = N_\pi, \tag{A7}$$

where $N_\pi = \Sigma_{l=1}^{L} N_l \delta\sigma_l$ includes the effect of advection of π by all the layer velocities. Vertical velocities at midlayers are derived from (A6) and (A7):

$$\dot{\sigma}_l = \frac{1}{2}(\dot{\sigma}_{l+1/2} + \dot{\sigma}_{l-1/2}) = \sigma_l \sum_{s=1}^{L} (\delta_s - N_s)\delta\sigma_s - \sum_{s=1}^{l-1} (\delta_s - N_s)\delta\sigma_s - \frac{1}{2}(\delta_l - N_l)\delta\sigma_l. \tag{A8}$$

We seek vertical normal modes of this set of equations. To derive these the temperature, mass and hydrostatic equations are combined into a single equation for **P**. For our purposes we wish the vertical modes to be orthogonal, which will introduce a constraint on the form of the a and b coefficients in the hydrostatic formula and on the form of the term representing the vertical advection of temperature. This is most easily demonstrated if we transfer all of the equations into matrix and vector form. Rewritten in this way the hydrostatic, temperature, and mass equation multiplied by $\bar{\mathbf{T}}$ are

$$\mathbf{\Phi} = \boldsymbol{\phi}_s + \mathbf{W}^{\mathrm{T}} T, \tag{A9}$$

$$\frac{\partial \mathbf{T}}{\partial t} + [\mathbf{\Gamma}(\mathbf{SE} - \mathbf{L}) + \mathbf{H}^{-1}\mathbf{KW}]\mathbf{H}\delta = \dot{\mathbf{R}}, \tag{A10}$$

$$\bar{\mathbf{T}} \frac{\partial \pi}{\partial t} + \mathbf{YEH}\delta = \bar{\mathbf{T}} N_\pi, \tag{A11}$$

where we have defined the following matrices:

$$\mathbf{W} = \begin{bmatrix} b_1 & 0 & & 0 \\ a_2 & b_2 & \ddots & 0 \\ & & & \\ a_L & a_L & & b_L \end{bmatrix},$$

$$\mathbf{K} = \mathrm{diag}[\kappa \bar{T}_l],$$

$$\mathbf{E} = [1],$$

$$\mathbf{H} = \mathrm{diag}[\delta\sigma_l],$$

$$\mathbf{S} = \mathrm{diag}[\sigma_l],$$

$$\mathbf{\Gamma} = \mathrm{diag}[(\bar{T}_{l+1/2} - \bar{T}_{l-1/2})/\delta\sigma_l],$$

$$\mathbf{Y} = \mathrm{diag}[\bar{T}_l], \tag{A12}$$

$$\mathbf{L} = \begin{bmatrix} \frac{1}{2} & 0 & & 0 \\ 1 & \frac{1}{2} & \ddots & 0 \\ & & & \\ 1 & 1 & & \frac{1}{2} \end{bmatrix}, \tag{A13}$$

and the vectors,

$$\dot{\mathbf{R}}^{\mathrm{T}} = [\dot{R}_1, \dot{R}_2, \cdots, \dot{R}_L],$$

$$\delta^{\mathrm{T}} = [\delta_1, \delta_2, \cdots, \delta_L].$$

We note that

$$\mathbf{Y} = \bar{T}_{L+1/2}\mathbf{I} - \mathbf{U\Delta}, \tag{A14}$$

where

$$\mathbf{U} = \mathbf{L}^{\mathrm{T}},$$

$$\Delta = \mathrm{diag}[(\bar{T}_{l+1/2} - \bar{T}_{l-1/2})]. \tag{A15}$$

From these equations, and using the definition of **P** in (A3), we can derive an equation for **P**

$$\frac{\partial \mathbf{P}}{\partial t} + [\mathbf{W}^{\mathrm{T}}\mathbf{H}^{-1}\mathbf{KW} + (\mathbf{W}^{\mathrm{T}}\mathbf{\Gamma S} - \mathbf{U\Delta})\mathbf{E} - \mathbf{W}^{\mathrm{T}}\mathbf{\Gamma L} + \bar{T}_{L+1/2}\mathbf{IE}]\mathbf{H}\delta = \mathbf{Q}. \tag{A16}$$

In the above, the **P** forcing **Q**, is given by

$$\mathbf{Q} = \mathbf{W}^{\mathrm{T}}\dot{\mathbf{R}} + \bar{\mathbf{T}} N_\pi. \tag{A17}$$

The matrix in square brackets on the left-hand side of (A16) is the vertical structure matrix. For its eigenvectors to be orthogonal (i.e., for the vertical normal modes of the model atmosphere to be orthogonal), it must be symmetric.

Since **H** and **K** are diagonal matrices, the first term is symmetric. Also, the last term is clearly symmetric. It can be shown that to ensure symmetry, $\mathbf{W}^{\mathrm{T}}\mathbf{\Gamma L}$ must be symmetric and $(\mathbf{W}^{\mathrm{T}}\mathbf{\Gamma S} - U\Delta) = 0$. If we set $\mathbf{W} = \mathbf{AL}$ with $\mathbf{A} = \mathrm{diag}[a_l]$ then $\mathbf{W}^{\mathrm{T}} = \mathbf{AU}$ and $\mathbf{W}^{\mathrm{T}}\mathbf{\Gamma L} = \mathbf{AU\Gamma L}$, which is seen to be symmetric. This (i.e., $\mathbf{W} = \mathbf{AL}$) requires that the hydrostatic coefficients obey $b_l = a_l/2$.

Next, making use of the fact that now $\mathbf{W}^{\mathrm{T}}\mathbf{\Gamma S} = \mathbf{AU\Gamma S}$, we require that

$$\mathbf{AU\Gamma S} = \mathbf{U\Delta}, \tag{A18}$$

or

$$\mathbf{\Gamma} = \mathbf{A}^{-1}\mathbf{\Delta S}^{-1}. \tag{A19}$$

This last equation implies

$$\Gamma_l = \frac{\bar{T}_{l+1/2} - \bar{T}_{l-1/2}}{a_l \sigma_l}. \tag{A20}$$

Using the definition of $\mathbf{\Gamma}$ in (A12) we conclude that

$$a_l = \delta\sigma_l/\sigma_l, \tag{A21}$$

$$b_l = \delta\sigma_l/2\sigma_l. \tag{A22}$$

We see that orthogonality of the vertical modes has forced a certain choice of vertical differencing of both the hydrostatic equation and the thermodynamic equation. This form of the differencing is conservative of energy but appears to prevent conservation of higher-order quantities. This is the reason why most GCMs and weather prediction models do not in fact have orthogonal vertical modes. That is, in most GCMs the vertical differencing has been chosen to conserve various quantities, but that choice also imposes nonorthog-

onality of the vertical modes. The modes used in initialization applications are in fact orthogonal approximations to the real vertical modes. After deriving this result, we became aware that Temperton (1984) and Kasahara and Shigehisa (1983) had already discussed the same point. The above derivation closely follows that of Temperton.

Define the vertical structure matrix $\mathbf{C}$ as

$$\mathbf{C} = (\mathbf{W}^T\mathbf{H}^{-1}\mathbf{K}\mathbf{W} - \mathbf{W}^T\mathbf{\Gamma}\mathbf{L} + \bar{T}_{L+1/2}\mathbf{I}\mathbf{E})\mathbf{H}. \quad \text{(A23)}$$

To find the vertical eigenfunctions and eigenvalues, we solve the system

$$\mathbf{C}\Psi = \Lambda\Psi, \quad \text{(A24)}$$

where

$$\Psi = [\psi_1\psi_2\cdots\psi_L], \quad \text{(A25)}$$

$$\Lambda = \text{diag}[\lambda_n]. \quad \text{(A26)}$$

That is, Ψ is the matrix whose columns are the vertical eigenvectors ψ_n, and Λ is a diagonal matrix whose diagonal elements are the eigenvalues of the vertical structure matrix $\mathbf{C}$. The equivalent depth that corresponds to the eigenvalue is given by λ_n/g. The orthogonality of the vertical modes is given by

$$\sum_{l=1}^{L} \psi_{ln}\psi_{lm}\delta\sigma_l = \begin{cases} 1, & \text{if } m = n \\ 0, & \text{if } m \neq n; \end{cases} \quad \text{(A27)}$$

u, v, and P are then expanded in terms of the vertical normal modes using

$$(\mathbf{u}, \mathbf{v}, \mathbf{P}) = \sum_{n=1}^{L} (u_n(\varphi, \mu), v_n(\varphi, \mu), P_n(\varphi, \mu))\psi_n(\sigma), \quad \text{(A28)}$$

$$(\mathbf{F}, \mathbf{G}, \mathbf{Q}) = \sum_{n=1}^{L} (F_n(\varphi, \mu), G_n(\varphi, \mu), Q_n(\varphi, \mu))\psi_n(\sigma). \quad \text{(A29)}$$

These can be substituted into (A1), (A2), and (A16) to give, after using the relation (A24) and the orthogonality condition (A27), a system of uncoupled two-dimensional shallow-water equations

$$\frac{\partial u_n}{\partial t} - \partial\Omega v_n + \frac{1}{a}(1-\mu^2)^{-1/2}\lambda_n^{1/2}\frac{\partial P_n'}{\partial\varphi} = F_n, \quad \text{(A30)}$$

$$\frac{\partial v_n}{\partial t} + \partial\Omega u_n + \frac{1}{a}(1-\mu^2)^{1/2}\lambda_n^{1/2}\frac{\partial P_n'}{\partial\mu} = G_n, \quad \text{(A31)}$$

$$\frac{\partial P_n'}{\partial t} + \lambda_n^{1/2}\delta_n = Q_n/\lambda_n^{1/2}. \quad \text{(A32)}$$

In the above $P_n' = \lambda_n^{-1/2}P_n$, a rescaling that proves useful in the horizontal expansion. We now have as many shallow-water systems as there are vertical modes. Following Kasahara (1976, 1978), we seek the normal modes of the shallow-water systems. The normal modes are known to be Hough functions, which are composed of infinite series of spherical harmonics. To find these modes, (A30) and (A31) are rewritten in terms of the velocity potential and streamfunctions. These two equations together with (A32) are expanded in terms of spherical harmonics $Y_s^m = P_s^m(\mu)e^{is\varphi}$, where P_s^m is an associated Legendre polynomial of the first kind. As shown by Kasahara, truncation of the spherical harmonic expansion at a zonal wavenumber S and associated Legendre polynomial P_S^M produces a matrix eigenvalue problem. The eigenvectors of the matrix contain the coefficients in the spherical harmonic expansion for the Hough modes of frequency given by the associated eigenvalue. Given these coefficients, horizontal normal-mode structures of velocity potential, streamfunction, and the pressure variable, P_n', for each Hough mode can be constructed. From these, structures of u and v can be constructed. Since u and v involve first-order derivatives of the streamfunction and velocity potential, a consistent formulation requires that their Legendre polynomial expansions be carried one order higher than the expansions of the streamfunction and velocity potential. The modes divide into westward and eastward moving gravity modes and Rossby modes and further divide into modes with u_n and P_n' symmetric about the equator or asymmetric about the equator. Whatever the spectral truncation, these Hough modes are guaranteed to be orthogonal for any equivalent depth. However, the coarser the truncation, the more the derived Hough modes depart from their continuous analogs. The treatment for the zonally symmetric geostrophic modes that appear within the system (and have zero frequency) is different from that for all other modes and is discussed by Kasahara (1978). The geostrophic modes can be made orthogonal to all the other modes despite their special form.

The truncation used in this model is arrived at by first deciding on the desired meridional resolution. This gives the number of grid points between the poles, J. If the grid points are placed optimally for the purposes of Gaussian quadrature, then integration of polynomials up to order $2J - 1$ can be performed exactly under Gaussian quadrature. Since assessment of orthogonality or projection of information onto the modes involves products of the mode structures, the highest-order associated Legendre polynomial we can retain, and guarantee exact integration for, is $J - 1$. This sets the value M in the spherical harmonic expansion. We choose $M = 59$ and $S = 32$, providing a gridpoint resolution of about 3×5.625. Hough mode structures of u_n, v_n, and P_n' are discretized onto this grid. They need to be computed only once for a given model setup and are then stored and read in at the beginning of each model run. The spectral truncation departs from both the traditional triangular ($M = S$) and rhomboidal ($M = S + K$, where K is another integer) truncations.

The horizontal eigenfunction expansion can be written

$$(u_n, v_n, P'_n) = \sum_{s=-S}^{s=S} \sum_{m=|s|}^{M} a_{smn} e^{is\varphi} (U_{smn}, V_{smn}, \tilde{P}'_{smn}), \tag{A33}$$

where U_{smn}, V_{smn}, and $\tilde{P}'_{smn}$ describe the meridional variations of u_n, v_n, and $\tilde{P}'_n$ for the Hough mode given by zonal wavenumber s, meridional index m, and vertical mode n. Here a_{smn} is the amplitude of the corresponding Hough mode. The orthogonality of the Hough modes for a given s and n is expressed as

$$\sum_{j=1}^{J} w_j (U_{smn} U^*_{sm'n} + V_{smn} V^*_{sm'n} + \tilde{P}'_{smn} \tilde{P}'^*_{sm'n}) = \begin{cases} 1, & \text{if } m = m' \\ 0, & \text{if } m \neq m', \end{cases} \tag{A34}$$

where the asterisk denotes complex conjugation, the w_j are weights that are required for exact Gaussian quadrature and the summation is over all grid points in the meridional direction. Orthogonality of modes with different zonal wavenumber is guaranteed by use of the Fourier expansion in the longitudinal direction. (Note that by redefining $V' = iV$ the whole system can be reduced to one in which the mode functions U, V', and $\tilde{P}'$ are real, saving storage and computation. In practice this is what we do, but we will continue to use the complex form in the following description.) Expanding (A30)–(A32) in this way reduces the shallow-water systems to the amplitude equation

$$\frac{da_{smn}}{dt} + i\sigma_{smn} a_{smn} = i f_{smn}. \tag{A35}$$

This equation can be solved analytically and without introduction of any phase error or computational dispersion of the linear wave components given the forcing f_{smn}. It is unconditionally stable whatever the time step used. The forcing is derived by projecting the forcing in physical space onto the normal-mode structures as follows:

$$f_{smn} = \sum_{j=1}^{J} w_j \frac{1}{2S} \sum_{i=1}^{2S} \sum_{l=1}^{L} (F(\varphi_i, \mu_j, \sigma_l) U_{smn}(\mu_j) + G(\varphi_i, \mu_j, \sigma_l) V_{smn}(\mu_j) + Q(\varphi_i, \mu_j, \sigma_l) \tilde{P}'_{smn}(\mu_j)/\lambda_n^{1/2}) \times \psi_n(\sigma_l) \delta\sigma_l e^{-is\varphi_i}; \tag{A36}$$

u, v, and P in physical space are given by

$$\begin{pmatrix} u(\varphi, \mu, \sigma) \\ v(\varphi, \mu, \sigma) \\ P(\varphi, \mu, \sigma) \end{pmatrix} = \sum_{n=1}^{L} \sum_{s=-S}^{S} \sum_{m=1}^{M} a_{smn} \begin{pmatrix} U_{smn} \\ V_{smn} \\ \lambda_n^{1/2} \tilde{P}'_{smn} \end{pmatrix} e^{is\varphi} \psi_m(\sigma). \tag{A37}$$

After the forcing has been projected onto the modes using (A36), the amplitudes of the modes calculated using (A35), and the physical space u, v, and P reconstructed using (A37), all that remains is to separate out the T and π contributions to P. From the equation for $\mathbf{P}$ given in (A16) with the definition of $\mathbf{C}$ in (A23), we can invert for δ and get

$$\delta = -\mathbf{C}^{-1} \frac{\partial \mathbf{P}}{\partial t} + \mathbf{C}^{-1} \mathbf{Q}, \tag{A38}$$

or, in scalar form,

$$\delta_l = -\sum_{j=1}^{L} C_{lj}^{-1} \frac{\partial P_j}{\partial t} + \sum_{j=1}^{L} C_{lj}^{-1} Q_j. \tag{A39}$$

The layer divergence in this form can be substituted into (A7) to get

$$\frac{\partial \pi}{\partial t} = \sum_{k=1}^{L} \delta\sigma_k \sum_{j=1}^{L} C_{kj}^{-1} \left(\frac{\partial P_j}{\partial t} - Q_j \right) + N_\pi. \tag{A40}$$

Here P is updated by solving the amplitude equation analytically for forcings held constant over the duration of the time step, Δt, from time n to time $n + 1$. Knowing P at the beginning and end of the time step and knowing the P and π forcing, we can solve for π as

$$\pi^{n+1} = \pi^n + \sum_{k=1}^{L} \delta\sigma_k \sum_{j=1}^{L} C_{kj}^{-1} (P_j^{n+1} - P_j^n - Q_j \Delta t) + N_\pi \Delta t. \tag{A41}$$

After π has been calculated we use (A3) to compute the geopotential:

$$\Phi = \mathbf{P} - R\bar{\mathbf{T}}\pi \tag{A42}$$

and finally invert the hydrostatic equation (A9) for temperature:

$$\mathbf{T} = (\mathbf{W}^{\mathrm{T}})^{-1} (\Phi - \phi_s). \tag{A43}$$

In the normal-mode initialization (NMI) literature the above derivation of the equations for π and T is often presented but with Q and N_π set to zero (e.g., Bourke and McGregor 1983; Temperton and Williamson 1981). This is the correct procedure to take when the initialization is linear but is also often used during nonlinear initialization when these forcing terms are definitely not zero. In nonlinear initialization (NNMI), modal amplitudes are adjusted so as to balance the nonlinear forcing with linear terms so as to zero the time tendency. The problem for the inverse vertical transform is that zeroing the time tendencies for the initialized modes means equations (A41) and (A38) are no longer valid. The change in P that initialization produced cannot be unambiguously separated into its π and T contributions. Daley (1979 and later papers) presented a variational method for dividing P into π and T contributions. More commonly the π and T adjustments are made in proportion to the P adjustments as

if the forcings were zero [see Errico (1991) for one of the few detailed discussions of this in the literature]. This does produce smooth fields of π and T. However, it is definitely the wrong procedure for time integration of a model. In the model, (A41) and (A38) are always valid, and hence the forced π equation (A41) is the one to use. There is no ambiguity in determining π or T in this case and the redundancy often mentioned in the initialization literature is absent here. However, inversion of P for π and T is an exacting test of the model. Any small error in the computed π leads to an error in ϕ that has the vertical structure of $\bar{T}$. When a ϕ proportional to $\bar{T}$ is inverted for T an oscillating vertical profile is retrieved. If done correctly such oscillations will not appear unless the forcing is very unrealistic. It is likely that one reason for retaining linear π and T inversion in NNMI is to avoid just this problem when π is poorly determined.

The model is filtered by eliminating from the system normal modes that have periods shorter than the time step since it is reasoned that these cannot be adequately represented within the model. This excludes many of the higher-frequency gravity waves.

As has been mentioned the model time integration scheme is unconditionally stable for any time step. In contrast, spectral models that use semi-implicit time integration schemes have limitations on their time step imposed by stability and accuracy considerations. The practical limitation on the time step here is the need to hold the forcing constant. Any forcing that operates on a time scale shorter than the time step will need to be parameterized so as to give forcings typical of an average over the length of the time step. We use a time step of one day and use a special treatment of processes such as convection that have shorter time scales. This affords a significant (order of magnitude) savings in computational expense relative to traditional spectral methods. By storing the mode structures on the model grid, no Legendre polynomial expansions or evaluations are required, which also affords savings of computer time. The reason why this normal-mode method has not been generally applied before seems to lie with the treatment of nonlinear advective terms. With traditional spectral models these terms are evaluated making use of the properties of spherical harmonics in a way that assures conservation of energy. The Hough mode representation used here affords no such advantage. We propose to use semi-Lagrangian methods for calculating advection that are in any case the only ones suitable for long time steps. It is notable that if semi-Lagrangian methods become more common within traditional spectral models, then the construction used here will be comparably more attractive even with use of a short time step. To our knowledge, this method has only been used by Daley (1980), who proposed such a scheme for the stable integration of fast gravity waves while treating slower waves with a time discretized scheme.

REFERENCES

Albrecht, B. A., A. K. Betts, W. H. Schubert, and S. K. Cox, 1979: A model of the thermodynamic structure of the trade wind boundary layer. Part I: Theoretical formulation and sensitivity tests. *J. Atmos. Sci.*, **36,** 73–89.

Arakawa, A., and W. H. Schubert, 1974: Interaction of a cumulus cloud ensemble with the large-scale environment, Part I. *J. Atmos. Sci.*, **31,** 674–701.

Betts, A. K., 1982: Saturation point analysis of moist convective overturning. *J. Atmos. Sci.*, **39,** 1484–1505.

——, 1986: A new convective adjustment scheme. Part I: Observational and theoretical basis. *Quart. J. Roy. Meteor. Soc.*, **112,** 677–691.

——, and M. J. Miller, 1986: A new convective adjustment scheme. Part II: Single column tests using GATE wave, BOMEX, ATEX and arctic air-mass data sets. *Quart. J. Roy. Meteor. Soc.*, **112,** 693–709.

——, and W. Ridgeway, 1988: Coupling of radiative, convective, and surface fluxes over the equatorial Pacific. *J. Atmos. Sci.*, **45,** 522–536.

Bladé, I., and D. L. Hartmann, 1993: Tropical intraseasonal oscillations in a simple nonlinear model. *J. Atmos. Sci.*, **50,** 2922–2939.

Bourke, W., and J. L. McGregor, 1983: A nonlinear vertical mode initialization scheme for a limited area prediction model. *Mon. Wea. Rev.*, **111,** 2285–2297.

Charney, J. G., 1971: Tropical cyclogenesis and the formation of the intertropical convergence zone. *Lectures in Applied Mathematics,* Vol. 13, W. Reid, Ed., Amer. Math. Soc., 355–369.

——, and A. Eliassen, 1964: On the growth of the hurricane depression. *J. Atmos. Sci.*, **21,** 68–75.

Corby, G. A., A. Gilchrist, and P. R. Rowntree, 1977: United Kingdom Meteorological Office five-level general circulation model. *Methods in Computational Physics,* Vol. 17, J. Chang, Ed., Academic Press, 67–109.

Daley, R., 1979: The application of non-linear normal mode initialization to an operational forecast model. *Atmos.–Ocean,* **17,** 97–124.

——, 1980: The development of efficient time integration schemes using model normal modes. *Mon. Wea. Rev.*, **108,** 100–110.

Emanuel, K. A., 1987: An air–sea interaction model of intraseasonal oscillations in the tropics. *J. Atmos. Sci.*, **44,** 2324–2340.

——, 1988: Reply. *J. Atmos. Sci.*, **45,** 3528–3530.

——, 1991: A scheme for representing cumulus convection in large-scale models. *J. Atmos. Sci.*, **48,** 2313–2335.

Errico, R. M., 1991: Theory and application of nonlinear normal mode initialization. Tech. Rep., NCAR/TN-344+IA, National Center for Atmospheric Research, Boulder, CO.

Fissel, D. B., S. Pond, and M. Miyake, 1977: Computation of surface fluxes from climatological and synoptic data. *Mon. Wea. Rev.*, **105,** 26–36.

Fu, R., A. D. Del Genio, and W. B. Rossow, 1990: Behavior of deep convective clouds in the tropical Pacific deduced from ISCCP radiances. *J. Climate,* **3,** 1129–1152.

Hayashi, Y.-Y., and A. Sumi, 1986: The 30–40 day oscillation in an 'aqua-planet' model. *J. Meteor. Soc. Japan II,* **64,** 451–467.

Hess, P. G., D. S. Battisti, and P. J. Rasch, 1993: Maintenance of the intertropical convergence zones and the large-scale tropical circulation on a water-covered earth. *J. Atmos. Sci.*, **50,** 691–713.

Holton, J. R., J. M. Wallace, and J. A. Young, 1971: On boundary layer dynamics and the ITCZ. *J. Atmos. Sci.*, **28,** 275–280.

Janjić, Z. I., 1990: The step-mountain coordinate: Physical passage. *Mon. Wea. Rev.*, **118,** 1429–1443.

Kasahara, A., 1976: Normal modes of ultralong waves in the atmosphere. *Mon. Wea. Rev.*, **104,** 669–690.

——, 1978: Further studies on a spectral model of the global barotropic primitive equations with Hough harmonic expansions. *J. Atmos. Sci.*, **35,** 2043–2051.

——, and Y. Shigehisa, 1983: Orthogonal vertical normal modes of a vertically staggered discretized atmospheric model. *Mon. Wea. Rev.*, **111,** 1724–1735.

Kuo, H.-L., 1974: Further studies of the influence of cumulus convection on large scale flow. *J. Atmos. Sci.,* **31,** 1232–1240.

Lau, K.-M., and L. Peng, 1987: Origin of low-frequency (intraseasonal) oscillations in the tropical atmosphere. Part I: Basic theory. *J. Atmos. Sci.,* **44,** 950–972.

Lau, N.-C., and K.-M. Lau, 1986: The structure and propagation of intraseasonal oscillations appearing in a GFDL general circulation model. *J. Atmos. Sci.,* **43,** 2023–2047.

——, I. M. Held, and J. D. Neelin, 1988: The Madden–Julian oscillation in an idealized general circulation model. *J. Atmos. Sci.,* **45,** 3810–3832.

Liu, W. T., K. B. Katsaros, and J. A. Businger, 1979: Bulk parameterization of air–sea exchange of heat and water vapor including molecular constraints at the interface. *J. Atmos. Sci.,* **36,** 1722–1735.

Miller, M. J., A. C. M. Beljaars, and T. N. Palmer, 1992: The sensitivity of the ECMWF model to the parameterization of evaporation from the tropical oceans. *J. Climate,* **5,** 418–434.

Neelin, J. D., and J.-Y. Yu, 1993: Modes of tropical variability under convective adjustment and the Madden–Julian Oscillation. Part I: Analytical theory. *J. Atmos. Sci.,* in press.

——, I. M. Held, and K. H. Cook, 1987: Evaporation–wind feedback and low-frequency variability in the tropical atmosphere. *J. Atmos. Sci.,* **44,** 2341–2348.

Ramanathan, V., and P. Downey, 1986: A nonisothermal emissivity and absorptivity formulation for water vapor. *J. Geophys. Res.,* **91,** 8649–8666.

Sarachik, E. S., 1978: Tropical sea surface temperature: An interactive one-dimensional model. *Dyn. Atmos. Oceans,* **2,** 455–469.

Schneider, E. K., and R. S. Lindzen, 1977: Axially symmetric steady-state models of the basic state for instability and climate studies. Part I: Linear calculations. *J. Atmos. Sci.,* **34,** 263–279.

Seager, R., 1991: A simple model of the climatology and variability of the low-level wind field in the tropics. *J. Climate,* **4,** 164–179.

Slingo, J., M. Blackburn, A. K. Betts, R. Brugge, B. Hoskins, M. J. Miller, L. Steenman-Clark, and J. Thuburn, 1993: Mean climate and transience in the tropics of the UGAMP GCM. Part I: Sensitivity to convective parameterization. Tech. Rep. 29, U.K. Universities Global Atmospheric Modelling Programme.

Soong, S.-T., and Y. Ogura, 1980: Response of trade wind cumuli to large-scale processes. *J. Atmos. Sci.,* **37,** 2035–2050.

Sui, C.-H., and K.-M. Lau, 1989: Origin of low-frequency (intraseasonal) oscillations in the tropical atmosphere. Part II: Structure and propagation of mobile wave–CISK modes and their modification by lower boundary forcings. *J. Atmos. Sci.,* **46,** 37–56.

Swinbank, R., T. N. Palmer, and M. K. Davey, 1988: Numerical simulations of the Madden and Julian Oscillation. *J. Atmos. Sci.,* **45,** 774–788.

Temperton, C., 1984: Orthogonal vertical normal modes for a multilevel model. *Mon. Wea. Rev.,* **112,** 503–509.

——, and D. L. Williamson, 1981: Normal mode initialization for a multilevel grid-point model. Part I: Linear aspects. *Mon. Wea. Rev.,* **109,** 729–743.

Weickmann, K. M., and S. J. S. Khalsa, 1990: The shift of convection from the Indian Ocean to the western Pacific Ocean during a 30–60 day oscillation. *Mon. Wea. Rev.,* **118,** 964–978.

Xu, K.-M., and K. A. Emanuel, 1989: Is the tropical atmosphere conditionally unstable? *Mon. Wea. Rev.,* **117,** 1471–1479.

Yano, J., and K. A. Emanuel, 1991: An improved model of the equatorial troposphere and its coupling with the stratosphere. *J. Atmos. Sci.,* **48,** 377–389.

Zebiak, S. E., 1986: Atmospheric convergence feedback in a simple model for El Niño. *Mon. Wea. Rev.,* **114,** 1263–1271.